

A Theory of the Inductive Bias and Generalization of Kernel Regression and Wide Neural Networks

James B. Simon¹ Madeline Dickens¹ Michael R. DeWeese¹

Abstract

Kernel regression is an important nonparametric learning algorithm with an equivalence to neural networks in the infinite-width limit. Understanding its generalization behavior is thus an important task for machine learning theory. In this work, we provide a theory of the inductive bias and generalization of kernel regression using a new measure characterizing the “learnability” of a given target function. We prove that a kernel’s inductive bias can be characterized as a fixed budget of learnability, allocated to its eigenmodes, that can only be increased with the addition of more training data. We then use this rule to derive expressions for the mean and covariance of the predicted function and gain insight into the overfitting and adversarial robustness of kernel regression and the hardness of the classic parity problem. We show agreement between our theoretical results and both kernel regression and wide finite networks on real and synthetic learning tasks.

1. Introduction

Kernel (ridge) regression — simply linear (ridge) regression with a kernel function replacing the standard dot product between data vectors — is an influential nonparametric learning algorithm with broad use across domains (de Vlaming & Groenen, 2015; Exterkate et al., 2016; Schulz et al., 2018). Theoretical interest in this algorithm has increased significantly in recent years due to the discovery that both Bayesian and trained neural networks converge to kernel regression in the infinite-width and infinite-time limit (Jacot et al., 2018; Lee et al., 2018), with one well-known paper declaring that “to understand deep learning we need to un-

derstand kernel learning” (Belkin et al., 2018). As relevant insights will elucidate both kernel regression and deep learning, understanding kernel regression is thus an important endeavor for the field of machine learning theory.

The most important desideratum of a learning algorithm is good generalization to unseen data. The generalization of deep neural networks remains mysterious, with a full quantitative theory still out of reach. Fortunately, Bordelon et al. (2020) made important progress towards understanding the generalization of kernel regression by deriving approximate analytical expressions for test mean-squared error (MSE) depending on the target function, kernel eigensystem, and training set size. Their final expressions quantify a spectral bias seen in many other studies: as points are added to the training set, higher eigenmodes are learned first.

However, that important study does not close the case on the theory of kernel regression for several reasons: (a) the authors provide no exact results, only approximations, and (b) there are many functionals of interest besides MSE. For example, the ability to also quantitatively predict the mean squared gradient $\mathbb{E}_x[|\nabla_x \hat{f}(x)|^2]$ for various domains and hyperparameters would be of clear use for the study of adversarial examples, which are essentially a phenomenon of surprisingly large gradient. Furthermore, (c) their derivations rely on heavy mathematical machinery, including a matrix PDE and replica calculations, that somewhat obscure the path to their main result, and (d) though they reveal that higher eigenmodes are better-learned, we find that there is a precise sense in which eigenmodes *compete* to be learned, which, to our knowledge, has not been described in any previous work.

1.1. Summary of Paper

In this work, we address points (a-d) with a new account of the generalization of kernel regression. To do so, we introduce two theoretical objects: the *learning transfer matrix* and a measure of generalization we call the *learnability* of the target function. The learning transfer matrix describes the action of the kernel regression operator in the kernel eigenbasis, transforming target eigencoefficients into predicted eigencoefficients, and is our principal object of study.

¹Department of Physics, Redwood Center for Theoretical Neuroscience, and Helen Wills Neuroscience Institute, University of California, Berkeley, Berkeley, CA 94720. Correspondence to: James B. Simon <james.simon@berkeley.edu>.

Code to reproduce all results available at <https://github.com/james-simon/eigenlearning>.

Learnability is the normalized inner product between the target and predicted functions. Learnability is intimately related to the bias term of the bias-variance decomposition of MSE and to the signal capture threshold of [Jacot et al. \(2020\)](#). We prove that, for kernel eigenmodes, it has several natural properties that MSE does not, including boundedness in $[0, 1]$ and monotonic improvement with training set size.

We begin by deriving several *exact* results describing these quantities and their dependence upon kernel eigenvalues. Our first main result (Theorem 3.2) is a conservation law describing the inductive bias of kernel regression: the sum of the learnabilities of any complete basis of target functions is at most the training set size. In the ridgeless case, this sum is exactly the training set size, *independent of the kernel*. This provides a concrete, intuitive picture of the design tradeoffs inherent in choosing a kernel: a kernel has a fixed budget of learnability it must divide among its eigenmodes.

We then use our framework to derive approximate expressions for the statistics of the predicted function. We make a set of approximations similar to those of [Bordelon et al. \(2020\)](#), but our derivation is quite different and uses only basic linear algebra. We derive expressions for both the mean and covariance of the target function (Theorem 4.1): in addition to recovering the expression for MSE of [Bordelon et al. \(2020\)](#), our results are sufficient to calculate other functionals of interest, such as the mean squared gradient. In concordance with the common notion of spectral bias, we find that a function is more learnable the more weight it places in higher-eigenvalue modes. We illustrate the power of our framework with a new result regarding the hardness of the parity problem for rotation-invariant kernels.

Along the way, we derive two results that shed light on the nature of overfitting in kernel regression. First, we prove that kernel regression necessarily generalizes with worse-than-chance MSE when attempting to learn a sufficiently low-learnability function, and that such a function always exists. Second, we show that, for modes below a certain eigenvalue threshold, MSE *increases* with additional samples in the small dataset regime because the model mistakenly explains them using more learnable modes. This phenomenon has appeared in the empirical results of other recent studies, but has never been explained.

We then run many experiments on real and synthetic datasets that corroborate our theoretical results. Using both kernel regression and wide, deep neural networks, we find excellent agreement with our theoretical predictions of the kernel conservation law, the first- and second-order statistics of the predicted function including the mean squared gradient, and overfitting at low dataset size. Finally, repeating one experiment with varying network width, we find good agreement even down to width 20, suggesting that kernel

eigenanalysis may be a fruitful approach even for the study of finite networks outside the kernel regime.

We conclude by discussing promising extensions and implications for the study of deep learning. The generalization of deep learning systems has long defied theoretical understanding, and even now there are few cases in which one can predict an interesting quantity or effect from first principles and then observe it in a deep learning experiment with excellent numerical agreement. These few well-understood cases are rare firm platforms on which future understanding can build. Our results provide several new well-understood quantities and phenomena regarding wide networks’ inductive bias, generalization, overfitting, and robustness, yielding new tools and insights for future studies.

1.2. Related Work

The generalization of kernel regression was first studied in the Gaussian process literature ([Sollich, 1999](#); [Vivarelli & Oppen, 1999](#); [Sollich, 2001](#)). These works typically assumed a restricted teacher-student framework, and none considered the problem in full generality.

[Jacot et al. \(2020\)](#) study the generalization of kernel ridge regression for positive ridge parameter using random matrix theory techniques. Their “reconstruction operator” is closely related to our learning transfer matrix, and their “signal capture threshold” ϑ is proportional to the constant t from [Bordelon et al. \(2020\)](#) and is the same as our constant C . They derive the mean predicted function and some, but not all, of its second-order statistics, a picture which our results complete.

[Canatar et al. \(2021\)](#) applied the work of [Bordelon et al. \(2020\)](#) to understanding certain generalization phenomena. One of their main insights is that learning curves can be nonmonotonic in the presence of zero eigenvalues and noise. Our overfitting results, though of a different nature, can be seen as generalizing this observation: we show that non-monotonic learning curves in fact require neither zero eigenvalues nor noise, only a sufficiently low eigenvalue.

The general observation that higher eigenmodes are easier learned appears in many recent works and is the essence of neural networks’ “spectral bias” towards simple functions ([Valle-Perez et al., 2018](#); [Yang & Salman, 2019](#)), which is apparent in both training speed ([Rahaman et al., 2019](#); [Xu et al., 2019b;a](#); [Xu, 2018](#); [Cao et al., 2019](#); [Su & Yang, 2019](#)) and generalization ([Arora et al., 2019](#)).

2. Theoretical Setup

2.1. Setting and Review of Kernel Regression

We consider the task of inferring an m -element function $f : \mathcal{X} \rightarrow \mathbb{R}^m$ given a set of n unique training points

$\mathcal{D} = \{x_i\}_{i=1}^n \subseteq \mathcal{X}$ and their corresponding function values $f(\mathcal{D}) \in \mathbb{R}^{n \times m}$. In the typical setting, data are drawn i.i.d. from a nonuniform distribution over a continuous \mathcal{X} . However, we find a much simpler analysis is possible if we instead consider a discrete problem that includes this setting as a limit: we let \mathcal{X} be discrete with cardinality $|\mathcal{X}| = M$ and assume the n samples are chosen randomly from \mathcal{X} without replacement. By taking $M \rightarrow \infty$ and allowing \mathcal{X} to fill a region of \mathbb{R}^d with nonuniform density, we can later recover the continuous limit.

Kernel regression is defined by the inference equation

$$\hat{f}(x) = K(x, \mathcal{D}) (K(\mathcal{D}, \mathcal{D}) + \delta \mathbf{I}_n)^{-1} f(\mathcal{D}), \quad (1)$$

where \hat{f} is the predicted function, $\delta \geq 0$ is the ridge parameter, $K : \mathcal{X} \times \mathcal{X} \rightarrow \mathbb{R}$ is the kernel function, $K(\mathcal{D}, \mathcal{D})$ is the “kernel matrix” with components $K(\mathcal{D}, \mathcal{D})_{ij} = K(x_i, x_j)$, and $K(x, \mathcal{D})$ is a row vector with components $K(x, \mathcal{D})_i = K(x, x_i)$.

Remarkably, for an infinite-width neural network trained to convergence on MSE loss, the predicted function is given by ridgeless kernel regression with the network’s “neural tangent kernel” (NTK) (Jacot et al., 2018; Lee et al., 2019). For unfamiliar readers, we define and motivate the NTK in Appendix B.

It follows from the form of Equation 1 that the m indices of f can each be treated separately: one can equivalently perform kernel regression on each index separately and simply vectorize the results. We thus hereafter assume $m = 1$ as the extension to $m > 1$ is trivial.

Given two functions g, h , we define their inner product to be $\langle g, h \rangle \equiv \mathbb{E}_{x \in \mathcal{X}}[g(x)h(x)]$, and we define the norm of a function g to be $\|g\|_2 \equiv \langle g, g \rangle^{1/2}$.

2.2. The Learning Transfer Matrix

We now translate Equation 1 into the eigenbasis of the kernel. Any kernel function must be symmetric and positive semidefinite (Shawe-Taylor et al., 2004), which implies that we can find a set of orthonormal eigenfunctions $\{\phi_i\}_{i=1}^M$ and nonnegative eigenvalues $\{\lambda_i\}_{i=1}^M$ that satisfy

$$\langle K(x, \cdot), \phi_i \rangle = \lambda_i \phi_i(x), \quad \langle \phi_i, \phi_j \rangle = \delta_{ij}. \quad (2)$$

We will assume for simplicity that K is positive *definite* and $\lambda_i > 0$, which will be true in most cases of interest.¹

We first decompose f and \hat{f} into weighted sums of the

¹We do not use the reproducing kernel Hilbert space (RKHS) formalism in this work, but we note that, by the Moore–Aronszajn theorem, the kernel K defines a unique RKHS.

eigenfunctions as

$$f(x) = \sum_{i=1}^M \mathbf{v}_i \phi_i(x), \quad \hat{f}(x) = \sum_{i=1}^M \hat{\mathbf{v}}_i \phi_i(x), \quad (3)$$

where \mathbf{v} and $\hat{\mathbf{v}}$ are vectors of coefficients. We note that $\langle f, \hat{f} \rangle = \mathbf{v}^T \hat{\mathbf{v}}$. As $K(x_1, x_2) = \sum_{i=1}^M \lambda_i \phi_i(x_1) \phi_i(x_2)$, we next decompose the kernel matrix as $K(\mathcal{D}, \mathcal{D}) = \Phi^T \Lambda \Phi$, where $\Phi_{ij} \equiv \phi_i(x_j)$ is the $M \times n$ “design matrix” and $\Lambda \equiv \text{diag}(\lambda_1, \dots, \lambda_M)$ is a diagonal matrix of eigenvalues.

The predicted coefficients $\hat{\mathbf{v}}$ are given by

$$\hat{v}_i = \langle \phi_i, \hat{f} \rangle = \lambda_i \phi_i(K(\mathcal{D}, \mathcal{D}) + \delta \mathbf{I}_n)^{-1} \Phi^T \mathbf{v}. \quad (4)$$

Stacking these coefficients into a matrix equation, we find

$$\hat{\mathbf{v}} = \Lambda \Phi (\Phi^T \Lambda \Phi + \delta \mathbf{I}_n)^{-1} \Phi^T \mathbf{v} = \mathbf{T}^{(\mathcal{D})} \mathbf{v}, \quad (5)$$

where the *learning transfer matrix* $\mathbf{T}^{(\mathcal{D})} \equiv \Lambda \Phi (\Phi^T \Lambda \Phi + \delta \mathbf{I}_n)^{-1} \Phi^T$ is an $M \times M$ matrix, independent of f , that fully describes the model’s learning behavior on a training set \mathcal{D} .

2.3. Learnability

We define the *learnability* of a target function f as

$$\mathcal{L}^{(\mathcal{D})}(f) \equiv \frac{\langle f, \hat{f} \rangle}{\|f\|_2^2}, \quad \mathcal{L}(f) \equiv \mathbb{E}_{\mathcal{D}} [\mathcal{L}^{(\mathcal{D})}(f)], \quad (6)$$

where $\mathcal{L}^{(\mathcal{D})}(f)$ (the “ \mathcal{D} -learnability”) is defined for a particular dataset and $\mathcal{L}(f)$ (the “learnability”) is its expectation over datasets. We analogously define \mathcal{D} -MSE and MSE as

$$\mathcal{E}^{(\mathcal{D})}(f) \equiv \|f - \hat{f}\|_2^2, \quad \mathcal{E}(f) \equiv \mathbb{E}_{\mathcal{D}} [\mathcal{E}^{(\mathcal{D})}(f)]. \quad (7)$$

Learnability is a peculiar quantity at first glance and deserves some motivation. It is of interest for several reasons:

- $\|f\|_2^2(1 - \mathcal{L}(f))^2$ is a lower bound for the bias term in the standard bias-variance decomposition of MSE (see Appendix D.4). Constraining learnability thus yields a bound on MSE.
- For kernel regression, learnability has several desirable properties that MSE does not. In particular, when f is an eigenfunction, it is bounded in $[0, 1]$ and only improves with the addition of more data (Lemma 3.1).
- Learnability obeys a conservation law and provides a useful way to view a kernel’s budget of inductive bias.
- Our approximate results can be expressed simply in terms of modewise learnabilities.

3. Exact Theoretical Results

We now present several exact results regarding learnability and the learning transfer matrix. All theoretical results henceforth are specialized to kernel regression. We relegate all proofs to Appendix D.

Lemma 3.1. *The following properties of $\mathbf{T}^{(\mathcal{D})}$, $\mathcal{L}^{(\mathcal{D})}$, \mathcal{L} , and $\{\phi_i\}_{i=1}^M$ hold:*

- (a) $\mathcal{L}^{(\mathcal{D})}(\phi_i) = \mathbf{T}_{ii}^{(\mathcal{D})}$, and $\mathcal{L}(\phi_i) = \mathbb{E}[\mathbf{T}_{ii}^{(\mathcal{D})}]$.
- (b) $\mathcal{L}(\phi_i), \mathcal{L}^{(\mathcal{D})}(\phi_i) \in [0, 1]$.
- (c) When $n = 0$, $\mathbf{T}^{(\mathcal{D})} = \mathbf{0}_M$ and $\mathcal{L}^{(\mathcal{D})}(f) = \mathcal{L}(f) = 0$.
- (d) When $n = M$ and $\delta = 0$, $\mathbf{T}^{(\mathcal{D})} = \mathbf{I}_M$ and $\mathcal{L}^{(\mathcal{D})}(f) = \mathcal{L}(f) = 1$.
- (e) Let \mathcal{D}_+ be $\mathcal{D} \cup x$, where $x \in X, x \notin \mathcal{D}$ is a new data point. Then $\mathcal{L}^{(\mathcal{D}_+)}(\phi_i) \geq \mathcal{L}^{(\mathcal{D})}(\phi_i)$.
- (f) $\frac{\partial}{\partial \lambda_i} \mathcal{L}^{(\mathcal{D})}(\phi_i) \geq 0$ and $\frac{\partial}{\partial \lambda_i} \mathcal{L}^{(\mathcal{D})}(\phi_j) \leq 0$.
- (g) $\frac{\partial}{\partial \delta} \mathcal{L}^{(\mathcal{D})}(\phi_i) \leq 0$.

Property (a) in Lemma 3.1 formalizes the relationship between the transfer matrix and learnability. Properties (b-e) together give an intuitive picture of the learning process: the learnability of each eigenfunction monotonically increases from zero as the training set grows, attaining its maximum of one in the ridgeless, maximal-data limit. Properties (f-g) show that the kernel eigenmodes are in competition: increasing one eigenvalue while fixing all others can only improve the learnability of the corresponding eigenfunction, but can only harm the learnabilities of all others. Property (h) shows that a ridge parameter only harms eigenfunction learnability.

We now present the conservation law obeyed by learnability.

Theorem 3.2 (Conservation of learnability). *For any complete basis of orthogonal functions \mathcal{F} , with zero ridge parameter,*

$$\sum_{f \in \mathcal{F}} \mathcal{L}^{(\mathcal{D})}(f) = \sum_{f \in \mathcal{F}} \mathcal{L}(f) = n, \quad (8)$$

and with positive ridge parameter,

$$\sum_{f \in \mathcal{F}} \mathcal{L}^{(\mathcal{D})}(f) < n \quad \text{and} \quad \sum_{f \in \mathcal{F}} \mathcal{L}(f) < n. \quad (9)$$

To understand the significance of this result, consider that one might naively hope to design a (neural tangent) kernel that achieves generally high performance for all target functions f . Theorem 3.2 states that this is impossible because,

averaged over a complete basis of functions, *all kernels achieve the same learnability*. Because there exist no universally high-performing kernels, we must instead aim to choose a kernel that assigns high learnability to task-relevant functions.

This result concretizes the notion of *inductive bias* for kernel regression. A learning algorithm’s inductive bias is the set of (implicit or explicit) assumptions about the nature of the target function that allow it to generalize to new data. As no algorithm can generalize well on all functions, an algorithm’s inductive bias is a design choice with inherent tradeoffs: enabling generalization on one subset of target functions typically means harming generalization on another.² For complex models used in practice, the inductive assumptions are highly implicit and the nature of these tradeoffs has long been unclear. By contrast, Theorem 3.2 makes these tradeoffs explicit, precisely characterizing a model’s inductive bias as a fixed budget of learnability it must divide among each set of orthogonal functions. The fact that this budget is exactly known (as opposed to being a bounded but unknown constant) will simplify our later derivations and allow us insight into the parity problem.

This theorem is similar in spirit to the classic “no-free-lunch” theorem for learning algorithms, which states that, averaged over *all* classification target functions, all models perform at chance level (Wolpert, 1996). However, Theorem 3.2 holds for *any orthogonal basis* of functions and thus gives a much stronger condition than the classic result. In subsequent derivations, we will choose this basis to be the eigenbasis.

A natural consequence of the bounded total learnability is that, if some functions are more learnable than average, others must be less. The following corollary states that, for these “losing” functions, the model *overfits*, and MSE evaluated off the training set is worse than that obtained by simply predicting zero.

Corollary 3.3 (Low- \mathcal{L} functions are overfit). *There is always a function for which $\mathcal{L}(f) \leq \frac{n}{M}$. If $\delta = 0$, the mean off-training-set MSE for any such function is at least as high as would be obtained by always predicting zero.*

It is, in some cases, intuitive that such a threshold exists: for example, a sufficiently-high-frequency function on a continuous input space will appear to be noise and will be overfit. However, it is perhaps surprising that even when learning a noiseless function on a finite input space, there must always be functions that are overfit.

²For example, choosing a linear model often leads to good performance on linear targets but poor performance on nonlinear targets.

4. Approximate Theoretical Results

We now obtain expressions for the mean and covariance of the learning transfer matrix and thus of the predicted function. Our derivation involves only basic linear algebra. We give the full derivation in Appendix E and sketch our method here. We first set the ridge parameter $\delta \rightarrow 0$, then take the following steps:

1. We observe that the only random variable is a design matrix Φ . The expectation is taken over many (i.e., $\frac{M!}{(M-n)!}$) such matrices, each obeying $\Phi^T \Phi = M\mathbf{I}_n$. We approximate this expectation with a continuous average over all Φ obeying this condition.
2. We show via symmetry that the off-diagonal elements of $\mathbb{E}[\mathbf{T}^{(\mathcal{D})}]$ are zero.
3. We show that the diagonal elements are given by

$$\mathbb{E}[\mathbf{T}_{ii}^{(\mathcal{D})}] = \mathbb{E}\left[\frac{\lambda_i}{\lambda_i + C_i^{(\mathcal{D})}}\right], \quad (10)$$

where $C_i^{(\mathcal{D})}$ is independent of λ_i . We argue that, in cases of interest, $C_i^{(\mathcal{D})}$ will concentrate around a mode-independent constant, so we replace it by its deterministic mean C .

4. Having fixed the form of $\mathbb{E}[\mathbf{T}^{(\mathcal{D})}]$, we fix the constant C using Theorem 3.2.
5. By taking a derivative of $\mathbf{T}^{(\mathcal{D})}$ w.r.t. Λ , we find the covariance of $\mathbf{T}^{(\mathcal{D})}$ with no additional approximations.
6. Noting that the ridge parameter can be seen essentially as a small increase to all eigenvalues, we immediately extend our results to nonzero ridge.

Our final expressions simplify if either $M \rightarrow \infty$ or $\delta = 0$ (to the same results in either limit), so we report these limits here and provide the general expressions in our derivations.

Theorem 4.1 (Statistics of the learning transfer matrix).

Under the above approximations, if either $M \rightarrow \infty$ or $\delta = 0$, the mean and covariance of the learning transfer matrix are given by

$$\mathbb{E}[\mathbf{T}_{ij}^{(\mathcal{D})}] = \delta_{ij} \mathcal{L}_i, \quad (11)$$

$$\text{Cov}[\mathbf{T}_{ij}^{(\mathcal{D})}, \mathbf{T}_{kl}^{(\mathcal{D})}] = \frac{\mathcal{L}_i(1 - \mathcal{L}_j)\mathcal{L}_k(1 - \mathcal{L}_\ell)}{n - \sum_{m=1}^M \mathcal{L}_m^2} \cdot (\delta_{ik}\delta_{j\ell} + \delta_{i\ell}\delta_{jk} - \delta_{ij}\delta_{k\ell}), \quad (12)$$

$$\text{where } \mathcal{L}_i \equiv \mathcal{L}(\phi_i) = \frac{\lambda_i}{\lambda_i + C} \quad (13)$$

$$\text{and } C \geq 0 \text{ satisfies } \sum_{i=1}^M \frac{\lambda_i}{\lambda_i + C} + \frac{\delta}{C} = n. \quad (14)$$

The learnability of an eigenfunction ϕ_i thus depends solely on the comparison of its eigenvalue to the constant C : if $\lambda_i \gg C$, the mode is learned, and if $\lambda_i \ll C$, it is not learned. As n grows, C monotonically decreases and makes successively lower eigenmodes learnable. This observation was also made by Jacot et al. (2020). In practice, Equation 14 can be numerically solved for C , but we also provide bounds on C in terms of $\{\lambda_i\}_i$ in Appendix E.8 as a tool for analytical study.

Under Theorem 4.1, the learnability of an arbitrary function is $\mathcal{E}(f) = \frac{1}{\sqrt{r}\sqrt{v}} \sum_i \mathbf{v}_i^2 \mathcal{L}_i$. A function is thus more learnable the more weight it places in high eigenvalue modes. As noted by Canatar et al. (2021), higher eigenmodes are typically simpler functions, and this bias towards high eigenmodes is the underlying explanation for (wide) neural networks' "spectral bias" towards low-frequency functions. However, we note that one can design a kernel with *complex* high eigenmodes (e.g. ?), and thus while spectral bias is merely a consequence of the kernels used in practice, the bias towards high eigenmodes is universal.

We extend these results to settings with target noise in Appendix E.7.

4.1. MSE and the Covariance of \hat{f}

Noting that $\mathcal{E}(f) = \mathbb{E}[|\mathbf{v} - \hat{\mathbf{v}}|^2]$, recalling that $\hat{\mathbf{v}} = \mathbf{T}^{(\mathcal{D})}\mathbf{v}$, and using Theorem 4.1 to evaluate a sum over eigenmodes, we recover the result of Bordelon et al. (2020) for expected MSE:

$$\mathcal{E}(f) = \frac{n}{n - \sum_m \mathcal{L}_m^2} \sum_i (1 - \mathcal{L}_i)^2 \mathbf{v}_i^2. \quad (15)$$

Taking a sum over indices of \mathbf{v} , we find that the covariance of the predicted function can be written simply in terms of MSE as³

$$\text{Cov}[\hat{\mathbf{v}}_i, \hat{\mathbf{v}}_j] = \frac{\mathcal{L}_i^2 \mathcal{E}(f)}{n} \delta_{ij}. \quad (16)$$

4.2. Learning Speeds and Double Descent

The denominator in Equation 12 and Equation 15 can also be written as $\sum_m \mathcal{L}_m(1 - \mathcal{L}_m) + \frac{\delta}{C}$. The quantity $\mathcal{L}_m(1 - \mathcal{L}_m)$ intuitively represents *the rate at which mode m is being learned*, as can be seen from the observation that

$$\frac{d\mathcal{L}_i}{dn} = \frac{\mathcal{L}_i(1 - \mathcal{L}_i)}{\sum_{m=1}^M \mathcal{L}_m(1 - \mathcal{L}_m) + \frac{\delta}{C}}. \quad (17)$$

This equation states that a new unit of learnability (i.e., a new data point) is split between all eigenmodes in proportion to $\mathcal{L}_i(1 - \mathcal{L}_i)$ (with a portion proportional to $\frac{\delta}{C}$ sacrificed to the ridge parameter).

$\mathcal{L}_m(1 - \mathcal{L}_m)$ is small for well- or poorly-learned modes and maximal when $\mathcal{L}_m = .5$. MSE is thus very high when all modes are either fully learned or not learned at all, which happens when the tail eigenvalues $\{\lambda_i\}_{i>n}$ are either zero or very small relative to $\{\lambda_i\}_{i\leq n}$. This is intimately related to the well-known double-descent phenomenon in which MSE peaks when the rank of the kernel equals n (Belkin et al., 2019; Mei & Montanari, 2019).

4.3. Mean Squared Gradient

Equations 11 and 12 for the statistics of the predicted function are important because they allow the prediction, and thus the theoretical study, of a wide array of functionals of \hat{f} for kernel regression and wide neural networks. There are many such functionals, and we admittedly cannot foresee which will prove most important; instead of having a narrow use case as motivation, we rather believe that the ability to predict generic 2nd-order statistics is a versatile new tool which is likely to have many applications.

That said, for concreteness, we highlight one such use case here. Adversarial examples are essentially a phenomenon of surprisingly large gradient, so the study of adversarial robustness would greatly benefit by the ability to study from first principles how problem parameters — e.g., data dimension, target function, and dataset size — affect the typical function gradient. One quantification of this, the *mean*

³Equation 71 in the supplement of Canatar et al. (2021) provides an expression for this covariance that, upon performing some algebra, agrees with ours except for a second, negative term proportional to $(1 - \delta_{ij})$. As $\mathcal{L}_i, \mathcal{L}_j \rightarrow 0$, the variance of $\hat{\mathbf{v}}_i, \hat{\mathbf{v}}_j$ approaches 0, but due to this additional term, the covariance approaches a finite negative value instead of 0, which is impossible. We thus believe that Equation 16 corrects this minor error.

squared gradient, is given by

$$\mathbb{E}_x \left[\left| \nabla_x \hat{f}(x) \right|^2 \right] = \sum_{ij} \mathbb{E}[\hat{\mathbf{v}}_i \hat{\mathbf{v}}_j] G_{ij}, \quad (18)$$

where $G_{ij} \equiv \mathbb{E}_x[\nabla_x \phi_i(x) \cdot \nabla_x \phi_j(x)]$, and can be predicted using Theorem 4.1.

4.4. Case Study: the Parity Problem

Setting aside the fact that Theorem 3.2 enabled a transparent new derivation of the statistics of \hat{f} , one might fairly question the value of our learnability framework as opposed to, e.g., the eigenvalue-centric approach of Bordelon et al. (2020). We demonstrate the power of our framework by using it to easily derive a new result regarding the hardness of the classic *parity problem*. The domain of this problem is the hypercube $\mathcal{X} = \{-1, +1\}^d$, over which we define the subset-parity functions

$$\phi_S(x) = (-1)^{\sum_{i \in S} \mathbb{1}[x_i=1]}, \quad (19)$$

where $S \subseteq \{1, \dots, d\} \equiv [d]$. The objective is to learn $\phi_{[d]}$. This was shown to be exponentially hard for Gaussian kernel methods by Bengio et al. (2006); here we extend this result to arbitrary rotation-invariant kernels.

For any rotation-invariant kernel, such as the NTK of a fully-connected neural network, $\{\phi_S\}_S$ are the eigenfunctions, with degenerate eigenvalues $\{\lambda_k\}_{k=0}^d$ depending only on $k = |S|$. Yang & Salman (2019) proved that, for any fully-connected kernel, the even and odd eigenvalues each obey an ordering in k . Letting d be odd for simplicity, this result and Equation 13 imply that $\mathcal{L}_1 \geq \mathcal{L}_3 \geq \dots \geq \mathcal{L}_d$. Counting level degeneracies, this is a hierarchy of 2^{d-1} learnabilities of which \mathcal{L}_d is the smallest. The conservation law of 3.2 then implies that

$$\mathcal{L}_d \leq \frac{n}{2^{d-1}}, \quad (20)$$

which, using the fact that $\mathcal{E} \geq (1 - \mathcal{L})^2$, implies that

$$\mathcal{E}(\phi_{[d]}) \geq \left(1 - \frac{n}{2^{d-1}}\right)^2. \quad (21)$$

Obtaining an MSE below a desired threshold ϵ thus requires at least $n_{\min} = 2^{d-1}(1 - \epsilon^{1/2})$ samples, which is exponential in d , our desired result. This analysis was made simple with our conservation law formulation, but is not at all obvious when MSE is written in terms of eigenvalues as in prior work.

4.5. Overfitting at Low n

Expanding an eigenfunction's MSE at low n , we find that $\mathcal{E}(\phi_i)|_{n=0} = 1$ and

$$\left. \frac{d\mathcal{E}(\phi_i)}{dn} \right|_{n=0} = \frac{1}{\sum_j \lambda_j + \delta} \left[\frac{\sum_j \lambda_j^2}{\sum_j \lambda_j + \delta} - 2\lambda_i \right]. \quad (22)$$

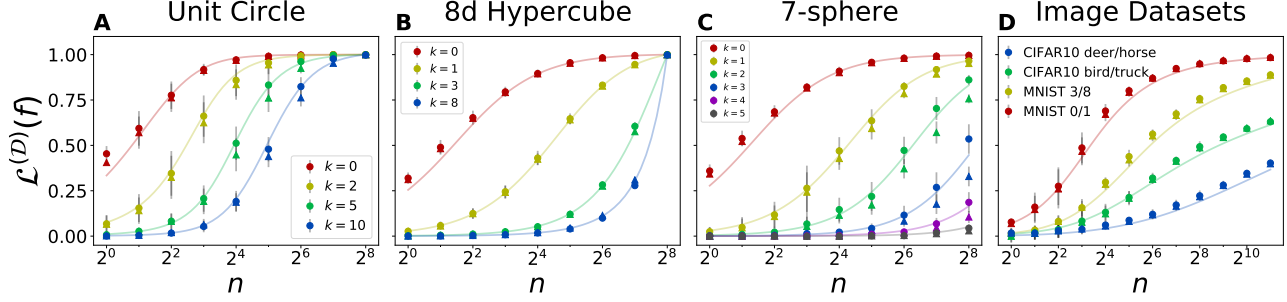


Figure 1: **Predicted learnabilities closely match experimental values.** (A-C) Each plot shows the learnability of several eigenfunctions on a synthetic domain. Theoretical predictions (curves) are plotted against experimental values from trained finite networks (circles) and NTK regression (triangles) with varying dataset size n . Error bars reflect 1σ variation due to random choice of dataset and, for finite nets, random initialization. (D) Predicted and experimental learnability for four binary image classification tasks.

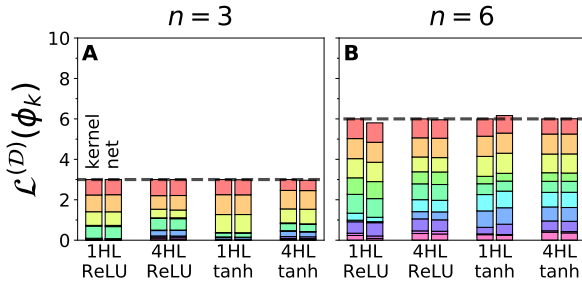


Figure 2: **Eigenfunction learnabilities always sum to the size of the training set.** Stacked bar charts with 10 components show \mathcal{D} -learnability for each of the 10 eigenfunctions on the unit circle discretized with $M = 10$. The left bar in each pair contains results from NTK regression, while the right bar contains results from trained finite networks. Dashed lines indicate n .

This implies that, at small n , MSE *increases* as samples are added for all modes i such that

$$\lambda_i < \frac{\sum_j \lambda_j^2}{2(\sum_j \lambda_j + \delta)}. \quad (23)$$

Because learnability (the projection of \hat{f} onto ϕ_i) is nonnegative, this worsening MSE is due to *overfitting*: confidently mistaking ϕ_i for more learnable modes. This expression confirms the intuitive expectation that increasing the ridge parameter tightens the eigenvalue threshold of Equation 23 and combats overfitting. This explains why MSE increases with n when learning difficult target functions in many of the experiments of Bordelon et al. (2020) and Misiakiewicz & Mei (2021), a fact which has not previously been explained. In studying MSE near $n = M$, Canatar et al. (2021) found a different class of increasing MSE curve, but they required both noise and a zero eigenvalue; by contrast, our observation is significantly more general, requiring only a sufficiently small eigenvalue.

5. Experimental Verification of Theoretical Results

We now perform experiments to confirm our various theoretical results for both ridgeless NTK regression and wide neural networks. Unless otherwise stated, all neural network experiments used a fully-connected (FC) four-hidden-layer (4HL) ReLU architecture with width 500 trained to convergence. We use the `neural_tangents` library (Novak et al., 2019) to perform NTK regression. Our experiments use both real image datasets and synthetic target functions on the following three domains.

1. *Discretized Unit Circle.* The simplest input space we consider is the discretization of the unit circle into M points, $\mathcal{X} = \{(\cos(2\pi j/M), \sin(2\pi j/M))\}_{j=1}^M$. Unless otherwise stated, we use $M = 256$. The eigenfunctions on this domain are $\phi_0(\theta) = 1$, $\phi_k(\theta) = \sqrt{2} \cos(k\theta)$, and $\phi'_k(\theta) = \sqrt{2} \sin(k\theta)$, for $k \geq 1$.
2. *Hypercube.* We also perform experiments on the d -dimensional hypercube, $\mathcal{X} = \{-1, 1\}^d$, giving $M = 2^d$. As stated in Section 4.4, the eigenfunctions on this domain are the subset-parity functions with eigenvalues determined by the number of sensitive bits k .
3. *Hypersphere.* To demonstrate that our results extend to continuous domains, we perform experiments on the d -sphere $\mathbb{S}^d \equiv \{x \in \mathbb{R}^{d+1} | x^2 = 1\}$. The eigenfunctions on this domain are the hyperspherical harmonics (see, e.g., Frye & Efthimiou (2012); Bordelon et al. (2020)) which group into degenerate sets indexed by $k \in \mathbb{N}$. The corresponding eigenvalues decrease exponentially with k , and so when summing over all eigenmodes when computing predictions, we simply truncate the sum at $k_{\max} = 70$.

Figure A.6 shows the eigenvalues for these domains as a function of k . On each domain, eigenvalues decrease essentially monotonically as k increases, in concordance with

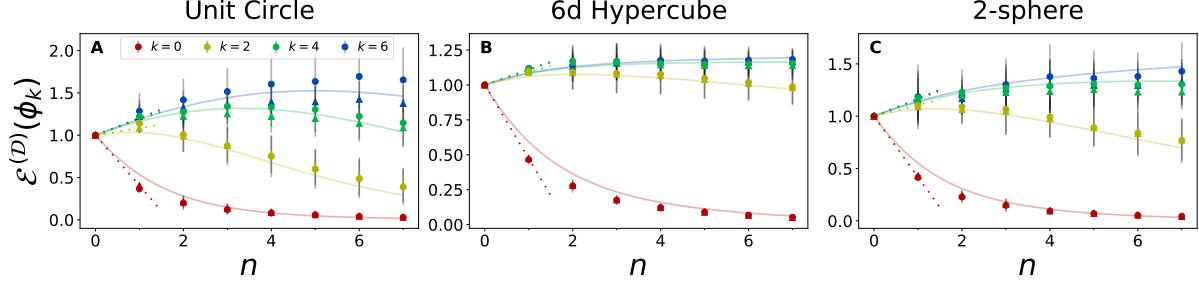


Figure 3: **For difficult eigenmodes, MSE increases with n due to overfitting.** Predicted MSE (curves) and empirical MSE for trained networks (circles) and NTK regression (triangles) for four eigenmodes on three domains at small n . Dotted lines indicated $d\mathcal{E}/dn|_{n=0}$ as predicted by Equation 22.

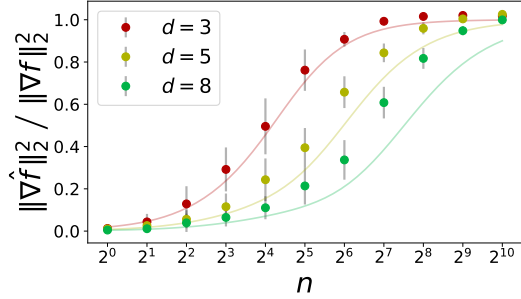


Figure 4: **Predicted mean squared gradient matches experiment.** Predicted mean squared gradient (curves) and empirical values for trained networks (circles) and kernel regression (triangles) for $k = 2$ modes on hyperspheres with $d \in \{3, 5, 8\}$, normalized by the ground-truth values.

the common intuition that neural nets are biased towards simple functions. Figure A.7 shows the eigenvalues and eigencoefficients for the binary image classification tasks used in our experiments.

Kernel conservation law. We first verify that total learnability equals the training set size. On the unit circle with $M = 10$, we train models on all 10 eigenfunctions with the same dataset \mathcal{D} and compute their resulting \mathcal{D} -learnabilities. Results are shown in Figure 2. We find that, for both shallow and deep models with both ReLU and tanh nonlinearities, the sum of modewise learnabilities equals n exactly for NTK regression and very nearly for trained networks.

Learnability. We next verify the predictions of Equation 13 for modewise learnability. We train 4HL models on several eigenmodes on each synthetic domain at varying n and compare predicted and empirical learnabilities in Figure 1(A-C). In all cases, we find excellent agreement between theory and experiment.

We also train 4HL models on four binary image classification tasks, generating theoretical predictions using 10^4 training samples as described in Appendix C. As shown in Figure 1D, not only do theoretical learnabilities match experimental learnabilities, but both match one’s intuitive expectation of the relative difficulty of these tasks, with MNIST

0/1 the most learnable pair and CIFAR10 deer/horse the least. In these cases, learnability is a useful metric for quantifying the difficulty of a task.

Furthermore, to evaluate the utility of $(1 - \mathcal{L})^2$ as a lower bound for MSE, we evaluate both quantities on these four image classification tasks. As shown in Figure A.8, we find that $(1 - \mathcal{L})^2$ is a remarkably close lower bound for MSE. This is important because it suggests that learnability, which we have shown is much simpler to study than MSE, can nonetheless furnish a faithful approximation for MSE in realistic settings.

Mean squared gradient. We next confirm that our results allow prediction of mean squared gradient (MSG) $\mathbb{E}_x[|\nabla_x \hat{f}(x)|^2] = \|\nabla \hat{f}\|_2^2$ as described in Section 4.3. On the hypersphere, the modewise gradient interaction constants are $G_{(k\ell), (k'\ell')} = k(k + d - 2)\delta_{kk'}\delta_{\ell\ell'}$. We train networks on modes with $k = 2$ with increasing dimension d and compute MSG on test data. Results are plotted in Figure 4.

Vulnerability to gradient-based adversarial attacks can be viewed essentially as a phenomenon of surprisingly large gradients. If such vulnerability is an inevitable consequence of high dimension, a common heuristic belief (e.g. Gilmer et al. (2018)), one should expect that MSG becomes much larger than the ground-truth value at high dimension. Surprisingly, we find no such effect. Our theory enables future first-principles study of this discrepancy.

Results for a comparable experiment on the unit circle, varying k instead of dimension, are shown in Figure A.9.

Increasing MSE curves. We next verify our prediction of increasing MSE curves for low eigenmodes as a result of overfitting. With small n , we fit four eigenmodes on each domain, three of which are predicted to have increasing MSE according to Equation 23. Our theoretical predictions match experiment excellently and match the true sign of $d\mathcal{E}/dn$ in every case.

Agreement with narrow networks. Our neural network experiments thus far have used moderately large widths

that place them in the NTK regime. However, realistic, finite-width networks are often not in the NTK regime and undergo significant kernel evolution and feature learning (Olah et al., 2017; Mei et al., 2018; Dyer & Gur-Ari, 2019; Yang & Hu, 2021). With typical network parameterization, the scale of these effects is controlled by network width, with more pronounced kernel evolution at narrower widths. It is thus important to study the finite-width deviations from our theory in order to gauge its scope of applicability.

To this end, we compute MSE and learnability for four hypercube eigenmodes using networks of widths from ∞ to 20. The results, plotted in Figure A.5, show that our predictions remain a good fit even down to width 20 for learnability and 50 for MSE. Furthermore, despite kernel evolution, the difficulty ordering of the target functions remains perfectly predicted by their eigenvalues with respect to the *infinite-width kernel*. These results strongly suggest that kernel eigenanalysis may prove a useful tool even for the study of the generalization of networks used in practice.

6. Conclusions

We have presented a new account of the generalization of kernel ridge regression using a new measure of target function learnability. This allowed us to describe the inductive bias of a kernel as a fixed budget of learnability, approximate the mean and covariance of the predicted function, obtain a new result regarding the hardness of the parity problem, and study network overfitting and robustness.

Our main results suggest many promising directions for future study, such as the comparison of convolutional and fully-connected architectures via eigenanalysis of their NTKs, the study of adversarial robustness using mean squared gradient, and the development of techniques to better apply our theory to real datasets. Our theory’s agreement with even fairly narrow networks is a surprise that may help guide theoretical endeavors to extend NTK analysis to finite width.

Acknowledgments

The authors thank Zack Weinstein for useful discussions and Chandan Singh, Sajant Anand, Jesse Livezey, Roy Rinberg, Jascha Sohl-Dickstein, and several reviewers for helpful comments on the manuscript. This research was supported in part by the U.S. Army Research Laboratory and the U.S. Army Research Office under contract W911NF-20-1-0151. JS gratefully acknowledges support from the National Science Foundation Graduate Fellow Research Program (NSF-GRFP) under grant DGE 1752814.

References

- Arora, S., Du, S., Hu, W., Li, Z., and Wang, R. Fine-grained analysis of optimization and generalization for overparameterized two-layer neural networks. In *International Conference on Machine Learning*, pp. 322–332. PMLR, 2019.
- Belkin, M., Ma, S., and Mandal, S. To understand deep learning we need to understand kernel learning. In *International Conference on Machine Learning*, pp. 541–549. PMLR, 2018.
- Belkin, M., Hsu, D., Ma, S., and Mandal, S. Reconciling modern machine-learning practice and the classical bias–variance trade-off. *Proceedings of the National Academy of Sciences*, 116(32):15849–15854, 2019.
- Bengio, Y., Delalleau, O., and Le Roux, N. The curse of highly variable functions for local kernel machines. *Advances in neural information processing systems*, 18: 107, 2006.
- Bordelon, B., Canatar, A., and Pehlevan, C. Spectrum dependent learning curves in kernel regression and wide neural networks. In *International Conference on Machine Learning*, pp. 1024–1034. PMLR, 2020.
- Bradbury, J., Frostig, R., Hawkins, P., Johnson, M. J., Leary, C., Maclaurin, D., Necula, G., Paszke, A., VanderPlas, J., Wanderman-Milne, S., and Zhang, Q. JAX: composable transformations of Python+NumPy programs, 2018. URL <http://github.com/google/jax>.
- Canatar, A., Bordelon, B., and Pehlevan, C. Spectral bias and task-model alignment explain generalization in kernel regression and infinitely wide neural networks. *Nature communications*, 12(1):1–12, 2021.
- Cao, Y., Fang, Z., Wu, Y., Zhou, D.-X., and Gu, Q. Towards understanding the spectral bias of deep learning. *arXiv preprint arXiv:1912.01198*, 2019.
- de Vlaming, R. and Groenen, P. J. The current and future use of ridge regression for prediction in quantitative genetics. *BioMed research international*, 2015, 2015.
- Del Ferraro, G., Wang, C., Martí, D., and Mézard, M. Cavity method: Message passing from a physics perspective. *arXiv preprint arXiv:1409.3048*, 2014.
- Dyer, E. and Gur-Ari, G. Asymptotics of wide networks from feynman diagrams. *arXiv preprint arXiv:1909.11304*, 2019.
- Exterkate, P., Groenen, P. J., Heij, C., and van Dijk, D. Nonlinear forecasting with many predictors using kernel ridge regression. *International Journal of Forecasting*, 32(3):736–753, 2016.

- Frye, C. and Efthimiou, C. J. Spherical harmonics in p dimensions. *arXiv preprint arXiv:1205.3548*, 2012.
- Gilmer, J., Metz, L., Faghri, F., Schoenholz, S. S., Raghu, M., Wattenberg, M., and Goodfellow, I. Adversarial spheres. *arXiv preprint arXiv:1801.02774*, 2018.
- Jacot, A., Hongler, C., and Gabriel, F. Neural tangent kernel: Convergence and generalization in neural networks. In *Advances in Neural Information Processing Systems (NeurIPS)*, pp. 8580–8589, 2018.
- Jacot, A., Şimşek, B., Spadaro, F., Hongler, C., and Gabriel, F. Kernel alignment risk estimator: risk prediction from training data. *arXiv preprint arXiv:2006.09796*, 2020.
- Lee, J., Bahri, Y., Novak, R., Schoenholz, S. S., Pennington, J., and Sohl-Dickstein, J. Deep neural networks as gaussian processes. In *International Conference on Learning Representations (ICLR)*. OpenReview.net, 2018.
- Lee, J., Xiao, L., Schoenholz, S. S., Bahri, Y., Novak, R., Sohl-Dickstein, J., and Pennington, J. Wide neural networks of any depth evolve as linear models under gradient descent. In *Advances in Neural Information Processing Systems (NeurIPS)*, pp. 8570–8581, 2019.
- Lewkowycz, A., Bahri, Y., Dyer, E., Sohl-Dickstein, J., and Gur-Ari, G. The large learning rate phase of deep learning: the catapult mechanism. *CoRR*, abs/2003.02218, 2020.
- Mei, S. and Montanari, A. The generalization error of random features regression: Precise asymptotics and the double descent curve. *Communications on Pure and Applied Mathematics*, 2019.
- Mei, S., Montanari, A., and Nguyen, P.-M. A mean field view of the landscape of two-layer neural networks. *Proceedings of the National Academy of Sciences*, 115(33): E7665–E7671, 2018.
- Misiakiewicz, T. and Mei, S. Learning with convolution and pooling operations in kernel methods. *arXiv preprint arXiv:2111.08308*, 2021.
- Novak, R., Xiao, L., Hron, J., Lee, J., Alemi, A. A., Sohl-Dickstein, J., and Schoenholz, S. S. Neural tangents: Fast and easy infinite neural networks in python. *CoRR*, abs/1912.02803, 2019.
- Olah, C., Mordvintsev, A., and Schubert, L. Feature visualization. *Distill*, 2(11):e7, 2017.
- Rahaman, N., Baratin, A., Arpit, D., Draxler, F., Lin, M., Hamprecht, F., Bengio, Y., and Courville, A. On the spectral bias of neural networks. In *International Conference on Machine Learning*, pp. 5301–5310. PMLR, 2019.
- Schulz, E., Speekenbrink, M., and Krause, A. A tutorial on gaussian process regression: Modelling, exploring, and exploiting functions. *Journal of Mathematical Psychology*, 85:1–16, 2018.
- Shawe-Taylor, J., Cristianini, N., et al. *Kernel methods for pattern analysis*. Cambridge university press, 2004.
- Sohl-Dickstein, J., Novak, R., Schoenholz, S. S., and Lee, J. On the infinite width limit of neural networks with a standard parameterization. *arXiv preprint arXiv:2001.07301*, 2020.
- Sollich, P. Learning curves for gaussian processes. *Advances in neural information processing systems*, pp. 344–350, 1999.
- Sollich, P. Gaussian process regression with mismatched models. *arXiv preprint cond-mat/0106475*, 2001.
- Spigler, S., Geiger, M., and Wyart, M. Asymptotic learning curves of kernel methods: empirical data versus teacher–student paradigm. *Journal of Statistical Mechanics: Theory and Experiment*, 2020(12):124001, 2020.
- Su, L. and Yang, P. On learning over-parameterized neural networks: A functional approximation perspective. *arXiv preprint arXiv:1905.10826*, 2019.
- Valle-Perez, G., Camargo, C. Q., and Louis, A. A. Deep learning generalizes because the parameter-function map is biased towards simple functions. *arXiv preprint arXiv:1805.08522*, 2018.
- Vivarelli, F. and Oppor, M. General bounds on bayes errors for regression with gaussian processes. *Advances in neural information processing systems*, 11:302–308, 1999.
- Wolpert, D. H. The lack of a priori distinctions between learning algorithms. *Neural computation*, 8(7):1341–1390, 1996.
- Xu, Z. J. Understanding training and generalization in deep learning by fourier analysis. *arXiv preprint arXiv:1808.04295*, 2018.
- Xu, Z.-Q. J., Zhang, Y., Luo, T., Xiao, Y., and Ma, Z. Frequency principle: Fourier analysis sheds light on deep neural networks. *arXiv preprint arXiv:1901.06523*, 2019a.
- Xu, Z.-Q. J., Zhang, Y., and Xiao, Y. Training behavior of deep neural network in frequency domain. In *International Conference on Neural Information Processing*, pp. 264–274. Springer, 2019b.

Yang, G. and Hu, E. J. Tensor programs iv: Feature learning in infinite-width neural networks. In *International Conference on Machine Learning*, pp. 11727–11737. PMLR, 2021.

Yang, G. and Salman, H. A fine-grained spectral perspective on neural networks. *arXiv preprint arXiv:1907.10599*, 2019.

A. Additional Figures

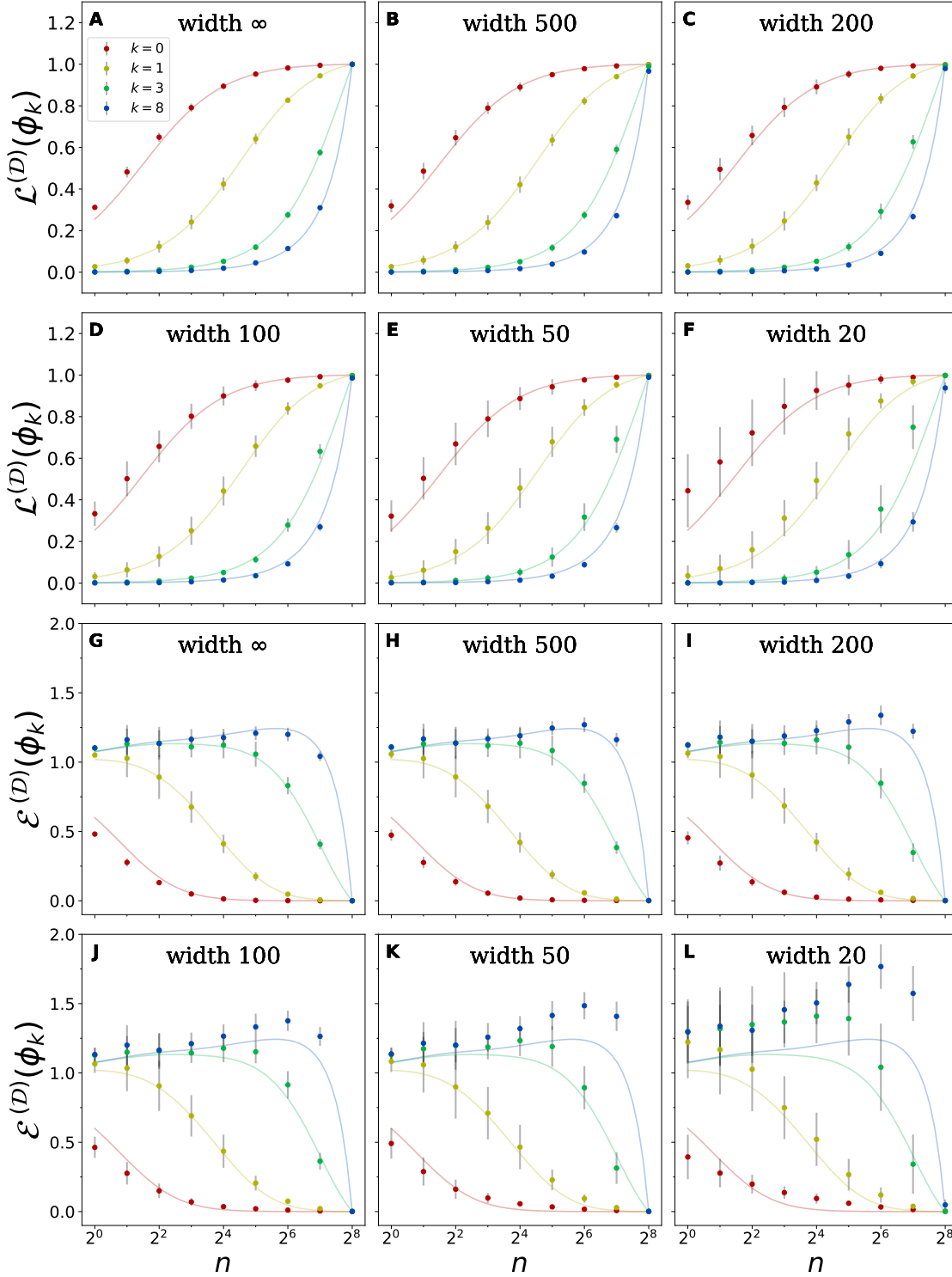


Figure A.5: **Comparison between predicted learnability and MSE for networks of various widths.** (A-F) Predicted (curves) and true (circles) learnability for four eigenmodes on the 8d hypercube. Dataset size n varies within each subplot, and the width of the 4HL ReLU network varies between subplots. (G-L) Same as (A-F) but with MSE instead of learnability.

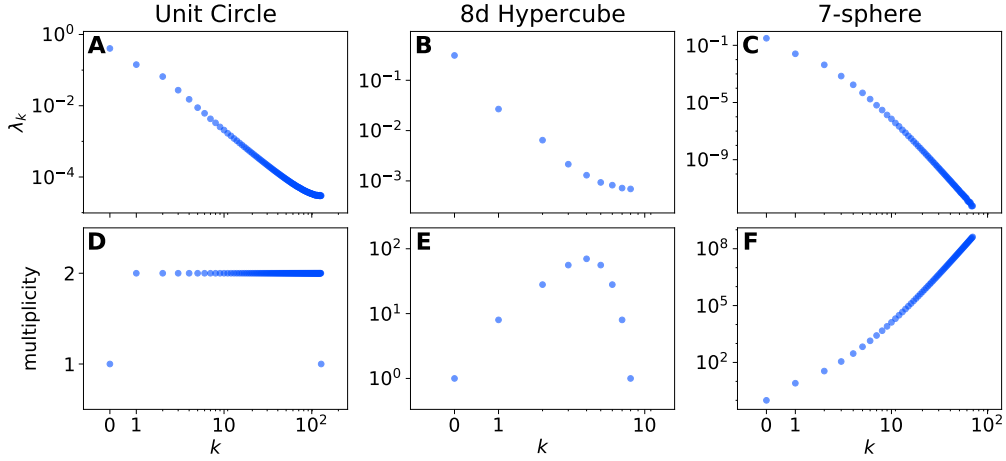


Figure A.6: **4HL ReLU NTK eigenvalues and multiplicities on three synthetic domains.** (A) Eigenvalues for k for the discretized unit circle ($M = 256$). Eigenvalues decrease as k increases except for a few near exceptions at high k . (B) Eigenvalues for the 8d hypercube. Eigenvalues decrease monotonically with k . (C) Eigenvalues for the 7-sphere up to $k = 70$. Eigenvalues decrease monotonically with k . (D) Eigenvalue multiplicity for the discretized unit circle. All eigenvalues are doubly degenerate (due to \cos and \sin modes) except for $k = 0$ and $k = 128$. (E) Eigenvalue multiplicity for the 8d hypercube. (F) Eigenvalue multiplicity for the 7-sphere.

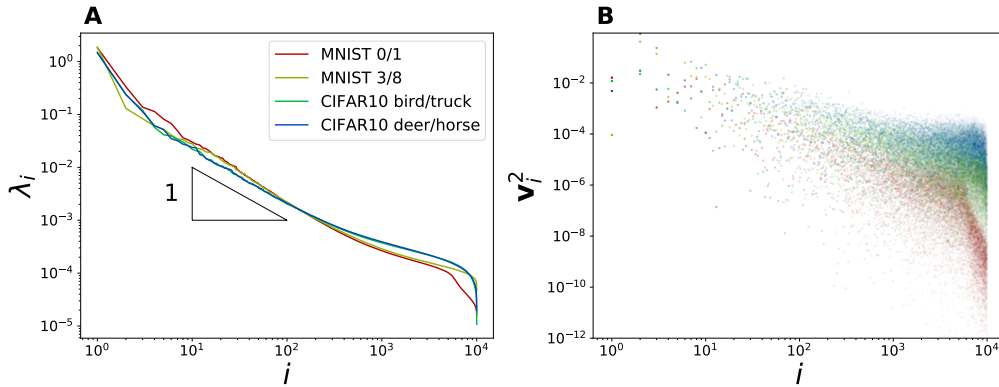


Figure A.7: **Eigenvalues and eigencoefficients for four binary image classification tasks.** (A) Kernel eigenvalues as computed from 10^4 training points as described in Appendix C. Spectra for CIFAR10 tasks roughly follow power laws with exponent -1 , while spectra for MNIST tasks follow power laws with slightly steeper descent. (B) Eigencoefficients as computed from 10^4 training points. Tasks with higher observed learnability (Figure 1) place more weight in higher (i.e., lower-index) eigenmodes and less in lower ones.

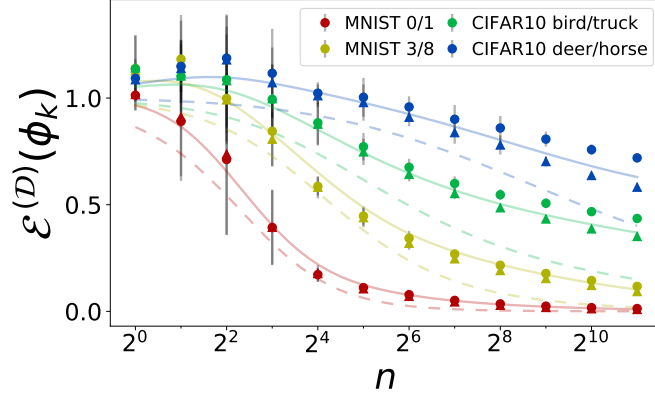


Figure A.8: **Learnability provides a close lower bound for MSE on image classification tasks.** Experimental MSE for finite networks (circles) and kernel regression (triangles), theoretical MSE (solid curves), and theoretical $(1 - \mathcal{L})^2$ (dashed curves) for four binary image classification tasks.

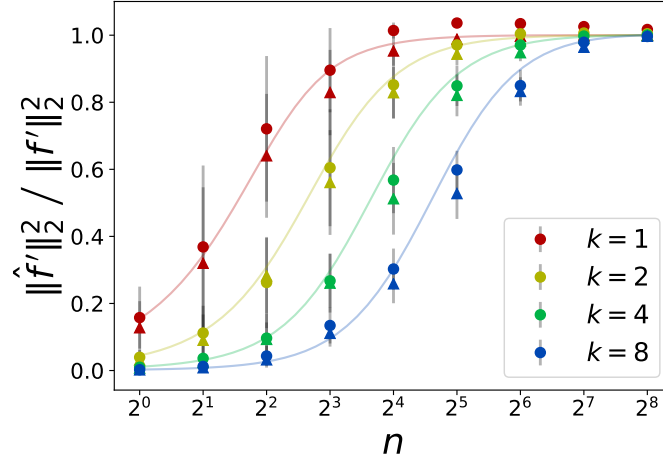


Figure A.9: **Predicted mean squared gradient matches experiment on the unit circle.** Mean squared gradient theoretical predictions (curves) and empirical values for finite networks (circles) and kernel regression (triangles) for various eigenmodes on the discretized unit circle with $M = 256$, normalized by the ground-truth mean squared gradient of $\mathbb{E}[|f'(x)|^2] = k^2$. Empirical values are computed discretely as $\mathbb{E}_j[|\hat{f}(x_j) - \hat{f}(x_{j+1})|^2]$, where x_j and x_{j+1} are neighboring points on the unit circle.

B. Review of the NTK

In the main text, we assume prior familiarity with the NTK, using Equation 1 as the starting point of our derivations. Here we provide a definition and very brief introduction to the NTK for unfamiliar readers. For derivations and full discussions, see Jacot et al. (2018) and Lee et al. (2019).

Consider a feedforward neural network representing a function $\hat{f}_\theta : \mathcal{X} \rightarrow \mathbb{R}$, where θ is a parameter vector. Further consider one training example x with target value y and one test point x' and suppose we perform one step of gradient descent with a small learning rate η with respect to the MSE loss $\ell_\theta \equiv (\hat{f}_\theta(x) - y)^2$. This gives the parameter update

$$\theta \rightarrow \theta + \delta\theta, \quad \text{with} \quad \delta\theta = -\eta \nabla_\theta \ell_\theta = -2\eta(\hat{f} - y) \nabla_\theta \hat{f}_\theta(x). \quad (24)$$

We now wish to know how this parameter update changes $\hat{f}_\theta(x')$. To do so, we linearize about θ , finding that

$$\begin{aligned}\hat{f}_{\theta+\delta\theta}(x') &= \hat{f}_\theta(x') + \nabla_\theta \hat{f}_\theta(x') \cdot \delta\theta + \mathcal{O}(\delta\theta^2) \\ &= \hat{f}_\theta(x') - 2\eta(\hat{f} - y) \left[\nabla_\theta \hat{f}_\theta(x) \cdot \nabla_\theta \hat{f}_\theta(x') \right] + \mathcal{O}(\delta\theta^2) \\ &= \hat{f}_\theta(x') - 2\eta(\hat{f} - y) K(x, x') + \mathcal{O}(\delta\theta^2),\end{aligned}\tag{25}$$

where we have defined $K(x, x') \equiv \nabla_\theta \hat{f}_\theta(x) \cdot \nabla_\theta \hat{f}_\theta(x')$. This quantity is the NTK. Remarkably, as network width⁴ goes to infinity, the $\mathcal{O}(\delta\theta^2)$ corrections become negligible, and $K(x, x')$ is the same after any random initialization⁵ and at any time during training. This dramatically simplifies the analysis of network training, allowing one to prove that after infinite time training on MSE loss for an arbitrary dataset, the network’s learned function is given by ridgeless kernel regression. See, for example, Equations 14-16 of Lee et al. (2019)⁶.

C. Experimental details

We conduct all our experiments using JAX (Bradbury et al., 2018), performing exact NTK regression with the `neural_tangents` library (Novak et al., 2019) built atop it. For the dataset sizes we consider in this paper, exact NTK regression is typically quite fast, running in seconds, while the training time of finite networks varies from seconds to minutes and depends on width, depth, training set size, and eigenmode. In particular, as described by Rahaman et al. (2019), lower eigenmodes take longer to train (especially when aiming for near-zero training MSE as we do here).

Naively, when training an infinitely-wide network, the NTK only describes the *mean* learned function, and the true learned function will include an NNGP-kernel-dependent fluctuation term reflecting the random initialization (Lee et al., 2019). However, by storing a copy of the parameters at $t = 0$ and redefining $\hat{f}_t(x) := \hat{f}_t(x) - \hat{f}_0(x)$ throughout optimization and at test time, this term becomes zero. We use this trick in our experiments with finite networks.⁷

Unless otherwise stated, all experiments used four-hidden-layer ReLU networks initialized with NTK parameterization (Sohl-Dickstein et al., 2020) with $\sigma_w = 1.4$, $\sigma_b = .1$. The tanh networks used in generating Figure 2 instead used $\sigma_w = 1.5$. Experiments on the unit circle always used a learning rate of .5, while experiments on the hypercube, hypersphere, and image datasets used a learning rate of .5 or .1 depending on the experiment. While higher learning rates led to faster convergence, they often also gave different generalization behavior, in line with the large learning rate regimes described by Lewkowycz et al. (2020). Means and 1σ error bars always reflect statistics from 30 random dataset draws and initializations (for finite nets), except for

- the learnability sum experiment of Figure 2, which used only a single trial,
- experiments on image datasets, which used 15 trials, and
- the nonmonotonic MSE curves of Figure 3, which used 100 trials.

Experiments with binary image classification tasks used scalar targets of ± 1 . To obtain the eigeninformation necessary for theoretical predictions, we examine a training set with 10^4 samples, computing the eigensystem of the data-data kernel matrix to obtain 10^4 eigenvalues $\{\lambda_i\}_i$ and projecting the target vector onto each eigenvector to compute a 10^4 -vector of target coefficients \mathbf{v} . We then compute theoretical learnability and MSE as normal.

These estimates turn out to be overly optimistic because our framework assumes that test data is drawn i.i.d. from the universe of M samples, and so if M is finite, then a particular test point has a n/M chance of belonging to the training set and being predicted perfectly. In our experiments (as in practice), however, this is not the case. We correct for this by

⁴The “width” parameter varies by architecture; for example it is the minimal hidden layer width for fully connected networks and the minimal number of channels per hidden layer for a convolutional network. Our theory holds for any architecture in the proper limit.

⁵(assuming the parameters are drawn from the same distribution)

⁶We note that there exists a different infinite-width kernel, called the “NNGP kernel,” describing a network’s random initialization, and this reference reserves \mathcal{K} for the NNGP kernel and uses Θ for the NTK.

⁷We credit this trick to a talk by Jascha Sohl-Dickstein.

computing the *off-training-set* learnability and MSE from the naive versions: subtracting off the free training set learnability and normalizing both quantities gives

$$\mathcal{L}_{\text{OTS}} = \frac{\mathcal{L}_{\text{naive}} - \frac{n}{M}}{1 - \frac{n}{M}}, \quad \mathcal{E}_{\text{OTS}} = \frac{\mathcal{E}_{\text{naive}}}{1 - \frac{n}{M}}. \quad (26)$$

We find the off-training-set quantities agree much better with experiment. It is these quantities that constitute the theoretical predictions in Figures 1 and A.8. Experimental quantities are computed with a random subset of 1500 images from the test set.

Bordelon et al. (2020) report similar experiments confirming their theoretical MSE on MNIST, but they allow duplicates and use knowledge of the test data in computing the eigensystem. By contrast, our predictions are generated strictly from training data (albeit from more than n samples). Applying kernel analysis to efficiently and accurately predict generalization performance on realistic data is an important problem, and as this comparison illustrates, there are many possible approaches.

D. Proofs: Exact Results

In this section, we provide proofs of the formal claims of Section 3. As a reminder, we note that

$$\mathbf{T}^{(\mathcal{D})} \equiv \mathbf{\Lambda} \mathbf{\Phi} (\mathbf{\Phi}^T \mathbf{\Lambda} \mathbf{\Phi} + \delta \mathbf{I}_n)^{-1} \mathbf{\Phi}^T. \quad (27)$$

We will also make use of the observation that the ridge parameter can be viewed essentially as a uniform increase in all eigenvalues. Letting $\mathbf{T}^{(\mathcal{D})}(\mathbf{\Lambda}; \delta)$ denote the learning transfer matrix with eigenvalue matrix $\mathbf{\Lambda}$ and ridge parameter δ , it follows from Equation 27 and the fact that $\mathbf{\Phi}^T \mathbf{\Phi} = M \mathbf{I}_n$ that

$$\mathbf{T}^{(\mathcal{D})}(\mathbf{\Lambda}; \delta) = \frac{\mathbf{\Lambda}}{\mathbf{\Lambda} + \frac{\delta}{M} \mathbf{I}_M} \mathbf{T}^{(\mathcal{D})} \left(\mathbf{\Lambda} + \frac{\delta}{M} \mathbf{I}_M; 0 \right). \quad (28)$$

D.1. Proof of Lemma 3.1 (Properties of $\mathbf{T}^{(\mathcal{D})}$, $\mathcal{L}^{(\mathcal{D})}$, and \mathcal{L})

Property (a): $\mathcal{L}^{(\mathcal{D})}(\phi_i) = \mathbf{T}_{ii}^{(\mathcal{D})}$, and $\mathcal{L}(\phi_i) = \mathbb{E}[\mathbf{T}_{ii}^{(\mathcal{D})}]$.

Proof. Using the fact that $\langle \phi_i, \phi_i \rangle = 1$, we see that $\mathcal{L}^{(\mathcal{D})}(\phi_i) = \langle \hat{\phi}_i, \phi_i \rangle = \mathbf{e}_i^T \mathbf{T}^{(\mathcal{D})} \mathbf{e}_i = \mathbf{T}_{ii}^{(\mathcal{D})}$, where \mathbf{e}_i is a one-hot M -vector with the one at index i . The second clause of the property follows by averaging.

Property (b): $\mathcal{L}(\phi_i), \mathcal{L}^{(\mathcal{D})}(\phi_i) \in [0, 1]$.

We observe that

$$\mathcal{L}^{(\mathcal{D})}(\phi_i) = \mathbf{e}_i^T \mathbf{T}^{(\mathcal{D})} \mathbf{e}_i \quad (29)$$

$$= \mathbf{e}_i^T \mathbf{\Lambda} \mathbf{\Phi} (\mathbf{\Phi}^T \mathbf{\Lambda} \mathbf{\Phi} + \delta \mathbf{I}_n)^{-1} \mathbf{\Phi}^T \mathbf{e}_i \quad (30)$$

$$= \text{Tr} \left[\mathbf{\Phi}^T \mathbf{e}_i \mathbf{e}_i^T \mathbf{\Lambda} \mathbf{\Phi} (\mathbf{\Phi}^T \mathbf{\Lambda} \mathbf{\Phi} + \delta \mathbf{I}_n)^{-1} \right] \leq 1, \quad (31)$$

$$(32)$$

where in the last line we have used the fact that

$$\mathbf{\Phi}^T \mathbf{\Lambda} \mathbf{\Phi} + \delta \mathbf{I}_n = \mathbf{\Phi}^T \mathbf{e}_i \mathbf{e}_i^T \mathbf{\Lambda} \mathbf{\Phi} + [\text{PSD matrix}], \quad (33)$$

which implies that the trace is less than or equal to one.

Property (c): When $n = 0$, $\mathbf{T}^{(\mathcal{D})} = \mathbf{0}_M$ and $\mathcal{L}^{(\mathcal{D})}(f) = \mathcal{L}(f) = 0$.

Proof. When $n = 0$, $\mathbf{\Phi}$ has no columns, and thus $\mathbf{T}^{(\mathcal{D})} = 0$. The other clauses follow from Property (a) and averaging.

Property (d): When $n = M$ and $\delta = 0$, $\mathbf{T}^{(\mathcal{D})} = \mathbf{I}_M$ and $\mathcal{L}^{(\mathcal{D})}(f) = \mathcal{L}(f) = 1$.

Proof. When $n = M$ and $\delta = 0$, Φ is a full-rank $M \times M$ matrix. Inspection of Equation 27 then shows that $\mathbf{T}^{(\mathcal{D})} = \mathbf{I}_M$. The other clauses follow from Property (a) and averaging.

Property (e): Let \mathcal{D}_+ be $\mathcal{D} \cup x$, where $x \in X, x \notin \mathcal{D}$ is a new data point. Then $\mathcal{L}^{(\mathcal{D}_+)}(\phi_i) \geq \mathcal{L}^{(\mathcal{D})}(\phi_i)$.

To begin, we set $\delta = 0$. We then use the Moore-Penrose pseudoinverse, which we denote by $(\cdot)^+$, to cast $\mathbf{T}^{(\mathcal{D})}$ into a more transparent form:

$$\mathbf{T}^{(\mathcal{D})} \equiv \mathbf{\Lambda} \Phi (\Phi^T \mathbf{\Lambda} \Phi)^{-1} \Phi^T = \mathbf{\Lambda}^{1/2} \left(\mathbf{\Lambda}^{1/2} \Phi \Phi^T \mathbf{\Lambda}^{1/2} \right) \left(\mathbf{\Lambda}^{1/2} \Phi \Phi^T \mathbf{\Lambda}^{1/2} \right)^+ \mathbf{\Lambda}^{-1/2}, \quad (34)$$

where we have suppressed the \mathcal{D} in $\Phi(\mathcal{D})$. This follows from the property of pseudoinverses that $\mathbf{A}(\mathbf{A}^T \mathbf{A})^+ \mathbf{A}^T = (\mathbf{A} \mathbf{A}^T)(\mathbf{A} \mathbf{A}^T)^+$ for any matrix \mathbf{A} . We now augment our system with one extra data point, getting

$$\mathbf{T}^{(\mathcal{D}_+)} = \mathbf{\Lambda}^{1/2} \left(\mathbf{\Lambda}^{1/2} (\Phi \Phi^T + \xi \xi^T) \mathbf{\Lambda}^{1/2} \right) \left(\mathbf{\Lambda}^{1/2} (\Phi \Phi^T + \xi \xi^T) \mathbf{\Lambda}^{1/2} \right)^+ \mathbf{\Lambda}^{-1/2}, \quad (35)$$

where ξ is an M -element column vector orthogonal to the others of Φ and satisfying $\xi^T \xi = M$. Equations 34 and 35 yield that

$$\mathcal{L}^{(\mathcal{D})}(\phi_i) = \mathbf{e}_i^T \mathbf{T}^{(\mathcal{D})} \mathbf{e}_i = \mathbf{e}_i^T \left(\mathbf{\Lambda}^{1/2} \Phi \Phi^T \mathbf{\Lambda}^{1/2} \right) \left(\mathbf{\Lambda}^{1/2} \Phi \Phi^T \mathbf{\Lambda}^{1/2} \right)^+ \mathbf{e}_i, \quad (36)$$

$$\mathcal{L}^{(\mathcal{D}_+)} = \mathbf{e}_i^T \mathbf{T}^{(\mathcal{D}_+)} \mathbf{e}_i = \mathbf{e}_i^T \left(\mathbf{\Lambda}^{1/2} (\Phi \Phi^T + \xi \xi^T) \mathbf{\Lambda}^{1/2} \right) \left(\mathbf{\Lambda}^{1/2} (\Phi \Phi^T + \xi \xi^T) \mathbf{\Lambda}^{1/2} \right)^+ \mathbf{e}_i. \quad (37)$$

The rightmost expressions of Equations 36 and 37 both contain a factor of the form $\mathbf{A} \mathbf{A}^+$, where \mathbf{A} is a positive semidefinite matrix. An operator of this form is a *projector* onto the row-space of \mathbf{A} . Comparing these equations, we find that the projectors are the same except that, in Equation 37, there is one additional dimension in the row-space and thus one new basis vector in the projector. This new basis vector can only increase $\mathbf{e}_i^T \mathbf{T}^{(\mathcal{D}_+)} \mathbf{e}_i$, and thus $\mathcal{L}^{(\mathcal{D}_+)}(\phi_i) \geq \mathcal{L}^{(\mathcal{D})}(\phi_i)$ in the ridgeless case.

This proof can easily be extended to nonzero ridge parameter using Equation 28, in which case Equations 36 and 37 both gain an overall factor of $\lambda_i / (\lambda_i + \frac{\delta}{M})$ and the same projector argument applies.

Property (f): $\frac{\partial}{\partial \lambda_i} \mathcal{L}^{(\mathcal{D})}(\phi_i) \geq 0$ and $\frac{\partial}{\partial \lambda_i} \mathcal{L}^{(\mathcal{D})}(\phi_j) \leq 0$.

Proof. Differentiating $\mathbf{T}_{jj}^{(\mathcal{D})}$ with respect to a particular λ_i , we find that

$$\frac{\partial}{\partial \lambda_i} \mathbf{T}_{jj}^{(\mathcal{D})} = (\delta_{ij} - \lambda_j \phi_j^T \mathbf{K}^{-1} \phi_i) \phi_i^T \mathbf{K}^{-1} \phi_j, \quad (38)$$

where ϕ_i^T is the i th row of Φ and $\mathbf{K} = \Phi^T \mathbf{\Lambda} \Phi + \delta \mathbf{I}_n$. Specializing to the case $i = j$, we note that $\phi_i^T \mathbf{K}^{-1} \phi_i \geq 0$ because \mathbf{K} is positive definite, and $\lambda_i \phi_i \mathbf{K}^{-1} \phi_i^T \leq 1$ because $\lambda_i \phi_i \phi_i^T$ is one of the positive semidefinite summands in $\mathbf{K} = \sum_k \lambda_k \phi_k \phi_k^T + \delta \mathbf{I}_n$. The first clause of the property follows.

To prove the second clause, we instead specialize to the case $i \neq j$, which yields that

$$\frac{\partial}{\partial \lambda_i} \mathbf{T}_{jj}^{(\mathcal{D})} = -\lambda_j \left(\phi_j^T \mathbf{K}^{-1} \phi_i \right)^2, \quad (39)$$

which is manifestly nonpositive because $\lambda_j > 0$. The desired property follows.

Property (g): $\frac{\partial}{\partial \delta} \mathcal{L}^{(\mathcal{D})}(\phi_i) \leq 0$.

Proof. Differentiating Equation 27 w.r.t. δ yields that $\frac{\partial}{\partial \delta} \mathbf{T}^{(\mathcal{D})} = -\mathbf{\Lambda} \Phi \mathbf{K}^{-2} \Phi^T$. We then observe that

$$\frac{\partial}{\partial \delta} \mathcal{L}^{(\mathcal{D})}(\phi_i) = \mathbf{e}_i^T \frac{\partial}{\partial \delta} \mathbf{T}^{(\mathcal{D})} \mathbf{e}_i = -\lambda_i \mathbf{e}_i^T \Phi \mathbf{K}^{-2} \Phi^T \mathbf{e}_i, \quad (40)$$

which must be nonpositive because $\lambda_i > 0$ and $\Phi \mathbf{K}^{-2} \Phi^T$ is manifestly positive definite. \square

We note that, in a prior version of this paper, properties (b), (e), and (g) were mistakenly written as applying to all target functions when they in fact apply only to eigenfunction.

D.2. Proof of Theorem 3.2 (Conservation of learnability)

First, we note that, for any orthogonal basis \mathcal{F} on \mathcal{X} ,

$$\sum_{f \in \mathcal{F}} \mathcal{L}^{(\mathcal{D})}(f) = \sum_{\mathbf{v} \in \mathcal{V}} \frac{\mathbf{v}^T \mathbf{T}^{(\mathcal{D})} \mathbf{v}}{\mathbf{v}^T \mathbf{v}}, \quad (41)$$

where \mathcal{V} is an orthogonal set of vectors spanning \mathbb{R}^M . This is equivalent to $\text{Tr}[\mathbf{T}^{(\mathcal{D})}]$. This trace is given by

$$\text{Tr}[\mathbf{T}^{(\mathcal{D})}] = \text{Tr}[\Phi^T \Lambda \Phi (\Phi^T \Lambda \Phi + \delta \mathbf{I}_n)^{-1}] = \text{Tr}\left[\frac{K}{K + \delta \mathbf{I}_n}\right]. \quad (42)$$

When $\delta = 0$, this trace simplifies to $\text{Tr}[\mathbf{I}_n] = n$. When $\delta > 0$, it is strictly less than n . This proves the theorem. \square

D.3. Proof of Corollary 3.3 (Low- \mathcal{L} Functions are Overfit)

It is an immediate consequence of the conservation law of Theorem 3.2 that any orthogonal basis of functions \mathcal{F} must contain an f such that $\mathcal{L}(f) \leq \frac{n}{M}$.

We now specialize to the case $\delta = 0$. In the ridgeless, kernel regression is an interpolating method, predicting exactly the training targets on any inputs that appear in the training set. Decomposing learnability as

$$\mathcal{L}(f) = \frac{1}{M \|f\|_2^2} \mathbb{E} \left[\sum_{x \in \mathcal{X}} f(x) \hat{f}(x) \right] = \frac{n}{M} + \frac{1}{M \|f\|_2^2} \mathbb{E} \left[\sum_{x \in \mathcal{X} \setminus \mathcal{D}} f(x) \hat{f}(x) \right], \quad (43)$$

we find that, for a function such that $\mathcal{L}(f) \leq \frac{n}{M}$, the second term is nonpositive.

Off-training-set (OTS) MSE is given by

$$\mathcal{E}_{\text{OTS}}(f) = \frac{1}{M - n} \mathbb{E} \left[\sum_{x \in \mathcal{X} \setminus \mathcal{D}} (f - \hat{f}(x))^2 \right] = \frac{1}{M - n} \mathbb{E} \left[\sum_{x \in \mathcal{X} \setminus \mathcal{D}} (f^2(x) - 2f(x)\hat{f}(x) + \hat{f}^2(x)) \right]. \quad (44)$$

If the model punts and predicts $\hat{f}(x) = 0$, OTS MSE is thus $\|f\|_2^2$. For a low-learnability function, the second and third terms are both nonnegative, yielding OTS MSE greater than or equal to this naive value. Examining the third term, unless the model does in fact always predict zero, its OTS MSE will be strictly greater. \square

D.4. Proof that $\mathcal{E}(f) \geq \|f\|_2^2(1 - \mathcal{L}(f))^2$

Here we show that knowing a particular function's learnability is sufficient to lower-bound the bias term of MSE (and thus for MSE itself). We will work with \mathbf{v} and $\hat{\mathbf{v}}$, the eigencoefficient vectors of f and \hat{f} . Expected MSE is given by

$$\mathcal{E}(f) = \mathbb{E}[(\mathbf{v} - \hat{\mathbf{v}})^2] = \mathbf{v}^2 - 2\mathbf{v}^T \mathbb{E}[\hat{\mathbf{v}}] + \mathbb{E}[\hat{\mathbf{v}}^2] = \underbrace{\mathbf{v}^2 - 2\mathbf{v}^T \mathbb{E}[\hat{\mathbf{v}}]}_{\text{bias}} + \underbrace{\mathbb{E}[\hat{\mathbf{v}}^2] - \mathbf{v}^2}_{\text{variance}}. \quad (45)$$

Projecting any vector onto an arbitrary unit vector can only decrease its magnitude, and so

$$\text{bias} \geq \mathbf{v}^2 - 2\mathbf{v}^T \mathbb{E}[\hat{\mathbf{v}}] + \mathbb{E}[\hat{\mathbf{v}}^T] \frac{\mathbf{v} \mathbf{v}^T}{|\mathbf{v}|^2} \mathbb{E}[\hat{\mathbf{v}}] = |\mathbf{v}|^2 \left(1 - \frac{\mathbf{v}^T \mathbb{E}[\hat{\mathbf{v}}]}{|\mathbf{v}|^2} \right)^2 = \|f\|_2^2 (1 - \mathcal{L}(f))^2. \quad (46)$$

This inequality is useful because it provides a bound on MSE in terms of learnability, which we show is simpler to study and obeys a conservation law. We use it in Section 4.4 to quickly show the difficulty of the parity problem.

E. Derivations: Approximate Results

In this section, we flesh out the derivation of the mean and covariance of $\mathbf{T}^{(\mathcal{D})}$ sketched in Section 4. We organize our derivation according to the steps outlined in the main text. We first derive our results with $\delta = 0$ and reintroduce a ridge parameter at the end.

E.1. Approximating Φ as a Random Matrix

Consider the $M \times M$ matrix $\tilde{\Phi}$ where $\tilde{\Phi}_{ij} = \phi_i(x_j)$ and the j index runs over the full input space \mathcal{X} . This matrix obeys $\tilde{\Phi}^T \tilde{\Phi} = \tilde{\Phi} \tilde{\Phi}^T = M \mathbf{I}_M$. The choice of a particular dataset amounts to the choice of n of these M rows to construct the design matrix Φ . Any such choice yields a Φ satisfying the orthonormalization condition $\Phi^T \Phi = M \mathbf{I}_n$.

Due to the large number of possible Φ , assuming no special structure in the eigenfunctions, it is reasonable to approximate it as a continuous average over all $M \times n$ matrices Φ such that $\Phi^T \Phi = M \mathbf{I}_n$ with the isotropic (Haar) measure. This approximation, which amounts to assuming no special structure in the eigenfunctions, is also made implicitly by [Bordelon et al. \(2020\)](#) and explicitly by [Jacot et al. \(2020\)](#).

E.2. Vanishing Off-Diagonals of $\mathbb{E}[\mathbf{T}^{(\mathcal{D})}]$

We next observe that

$$\mathbb{E}_{\Phi} \left[\Lambda \Phi (\Phi^T \mathbf{U}^T \Lambda \mathbf{U} \Phi)^{-1} \Phi^T \right] = \mathbb{E}_{\Phi} \left[\Lambda \mathbf{U}^T \Phi (\Phi^T \Lambda \Phi)^{-1} \Phi^T \mathbf{U} \right], \quad (47)$$

where \mathbf{U} is any orthogonal $M \times M$ matrix. Defining $\mathbf{U}^{(m)}$ as the matrix such that $\mathbf{U}_{ab}^{(m)} \equiv \delta_{ab}(1 - 2\delta_{am})$, noting that $\mathbf{U}^{(m)} \Lambda \mathbf{U}^{(m)} = \Lambda$, and plugging $\mathbf{U}^{(m)}$ in as \mathbf{U} in Equation 47, we find that

$$\mathbb{E} \left[\mathbf{T}_{ab}^{(\mathcal{D})} \right] = \left(\left(\mathbf{U}^{(m)} \right)^T \mathbb{E} \left[\mathbf{T}^{(\mathcal{D})} \right] \mathbf{U}^{(m)} \right)_{ab} = (-1)^{\delta_{am} + \delta_{bm}} \mathbb{E} \left[\mathbf{T}_{ab}^{(\mathcal{D})} \right]. \quad (48)$$

By choosing $m = a$, we conclude that $\mathbb{E} \left[\mathbf{T}_{ab}^{(\mathcal{D})} \right] = 0$ if $a \neq b$.

E.3. Fixing the Form of $\mathbb{E}[\mathbf{T}_{ii}^{(\mathcal{D})}]$

E.3.1. ISOLATING THE DESIRED ELEMENT

We now isolate a particular diagonal element of the mean learning transfer matrix. To do so, we write $\mathbb{E} \left[\mathbf{T}_{ii}^{(\mathcal{D})} \right]$ in terms of λ_i (the i th eigenvalue), $\Lambda_{(i)}$ (Λ with its i th row and column removed), ϕ_i^T (the i th row of Φ), and $\Phi_{(i)}$ (Φ with its i th row removed). Using the Sherman-Morrison matrix inversion formula, we find that

$$\begin{aligned} (\Phi^T \Lambda \Phi)^{-1} &= \left(\Phi_{(i)}^T \Lambda_{(i)} \Phi_{(i)} + \lambda_i \phi_i \phi_i^T \right)^{-1} \\ &= \left(\Phi_{(i)}^T \Lambda_{(i)} \Phi_{(i)} \right)^{-1} - \frac{\lambda_i \left(\Phi_{(i)}^T \Lambda_{(i)} \Phi_{(i)} \right)^{-1} \phi_i \phi_i^T \left(\Phi_{(i)}^T \Lambda_{(i)} \Phi_{(i)} \right)^{-1}}{1 + \lambda_i \phi_i^T \left(\Phi_{(i)}^T \Lambda_{(i)} \Phi_{(i)} \right)^{-1} \phi_i}. \end{aligned} \quad (49)$$

Inserting this into the expectation of $\mathbf{T}^{(\mathcal{D})}$, we find that

$$\begin{aligned}
 \mathbb{E}[\mathbf{T}_{ii}^{(\mathcal{D})}] &= \mathbb{E}_{\Phi_{(i)}, \phi_i} \left[\lambda_i \phi_i^T \left(\Phi_{(i)}^T \Lambda_{(i)} \Phi_{(i)} \right)^{-1} \phi_i - \frac{\lambda_i^2 \left[\phi_i^T \left(\Phi_{(i)}^T \Lambda_{(i)} \Phi_{(i)} \right)^{-1} \phi_i \right]^2}{1 + \lambda_i \phi_i^T \left(\Phi_{(i)}^T \Lambda_{(i)} \Phi_{(i)} \right)^{-1} \phi_i} \right] \\
 &= \mathbb{E}_{\Phi_{(i)}, \phi_i} \left[\frac{\lambda_i}{\lambda_i + \left[\phi_i^T \left(\Phi_{(i)}^T \Lambda_{(i)} \Phi_{(i)} \right)^{-1} \phi_i \right]^{-1}} \right] \\
 &= \mathbb{E}_{\Phi_{(i)}, \phi_i} \left[\frac{\lambda_i}{\lambda_i + C(\Phi_{(i)}, \phi_i)} \right],
 \end{aligned} \tag{50}$$

where $C(\Phi_{(i)}, \phi_i) \equiv C_i^{(\Phi)} \equiv \left[\phi_i^T \left(\Phi_{(i)}^T \Lambda_{(i)} \Phi_{(i)} \right)^{-1} \phi_i \right]^{-1}$ is a nonnegative scalar.

E.3.2. CONCENTRATION OF $C_i^{(\Phi)}$

We now argue that, in realistic settings, $C_i^{(\Phi)}$ concentrates about its deterministic mean $C_i \equiv \mathbb{E}[C_i^{(\Phi)}]$. This simply requires observing that, if $C_i^{(\Phi)}$ were to have significant variance relative to its mean, then for modes i such that $\lambda_i \sim C_i^{(\Phi)}$, $\mathbf{T}_{ii}^{(\mathcal{D})}$ and thus $\mathcal{L}^{(\mathcal{D})}(\phi_i)$ would also vary significantly with random dataset selection. However, as with most generalization metrics, we should in general expect that in realistic settings, simply resampling the dataset will not drastically change the resulting \mathcal{D} -learnability. In order for \mathcal{D} -learnability to have the expected small fluctuations, $C_i^{(\Phi)}$ must concentrate. Our experimental results in Figure 1 confirm that these fluctuations are indeed small in practice, especially at large n .

E.3.3. MODE-INDEPENDENCE OF C_i

We next argue that C_i is approximately independent of i , so we can replace it with a constant C . This requires another natural assumption: adding one additional eigenmode does not significantly change the (mean) learnability of a particular eigenmode. We expect this to hold true for realistic eigenspectra at modestly large n , at which adding one additional sample (i.e. one additional unit of learnability) also does not significantly change $\mathcal{L}(\phi_i)$.⁸ In particular, we assume that

$$\mathbb{E}[\mathbf{T}_{ii}^{(\mathcal{D})}] \approx \frac{\lambda_i}{\lambda_i + C_i} \approx \frac{\lambda_i}{\lambda_i + C_i^+} \implies C_i \approx C_i^+, \tag{51}$$

where C_i^+ is C_i computed with the addition of another eigenmode. We choose the additional eigenmode to have eigenvalue λ_i , and we insert it at index i , effectively reinserting the missing mode i into $\Phi_{(i)}$ and $\Lambda_{(i)}$.

To clarify the random variables in play, we shall adopt a more explicit notation, writing out $\Phi_{(i)}$ in terms of its row vectors as $\Phi_{(i)} = [\phi_1, \dots, \phi_{i-1}, \phi_{i+1}, \dots, \phi_M]^T$. Using this notation, we find upon adding the new eigenmode that

$$C_i \equiv \mathbb{E}_{\Phi_{(i)}, \phi_i} \left[\left[\phi_i^T \left(\Phi_{(i)}^T \Lambda_{(i)} \Phi_{(i)} \right)^{-1} \phi_i \right]^{-1} \right] \tag{52}$$

$$\equiv \mathbb{E}_{\{\phi_k\}_{k=1}^M} \left[\left[\phi_i^T \left([\phi_1, \dots, \phi_{i-1}, \phi_{i+1}, \dots, \phi_M] \Lambda_{(i)} [\phi_1, \dots, \phi_{i-1}, \phi_{i+1}, \dots, \phi_M]^T \right)^{-1} \phi_i \right]^{-1} \right] \tag{53}$$

$$\approx C_i^+ \equiv \mathbb{E}_{\{\phi_k\}_{k=1}^M, \tilde{\phi}_i} \left[\left[\phi_i^T \left([\phi_1, \dots, \phi_{i-1}, \tilde{\phi}_i, \phi_{i+1}, \dots, \phi_M] \Lambda [\phi_1, \dots, \phi_{i-1}, \tilde{\phi}_i, \phi_{i+1}, \dots, \phi_M]^T \right)^{-1} \phi_i \right]^{-1} \right], \tag{54}$$

⁸There are certainly pathological eigenspectra that will violate this assumption for a particular mode. For example, given an eigenspectrum with a large gap between $\lambda_{\ell-1}$ and λ_ℓ , the learnability of mode ℓ when $n = \ell$ will be greatly affected by the insertion of an additional high-eigenvalue mode. However, as kernel eigenspectra are typically well-behaved in practice (and even in the worst case most eigenmodes will not be thus susceptible), this assumption is reasonable.

where $\mathbf{\Lambda}$ is the original eigenvalue matrix and $\tilde{\phi}_i^T$ is the design matrix row corresponding to the new mode.

We can also perform the same manipulation with C_j , this time adding an additional eigenvalue λ_j at index j , yielding that

$$C_j \equiv \mathbb{E}_{\Phi_{(j)}, \phi_j} \left[\left[\phi_j^T \left(\Phi_{(j)}^T \mathbf{\Lambda}_{(j)} \Phi_{(j)} \right)^{-1} \phi_j \right]^{-1} \right] \quad (55)$$

$$\equiv \mathbb{E}_{\{\phi_k\}_{k=1}^M} \left[\left[\phi_j^T \left([\phi_1, \dots, \phi_{j-1}, \phi_{j+1}, \dots, \phi_M] \mathbf{\Lambda}_{(j)} [\phi_1, \dots, \phi_{j-1}, \phi_{j+1}, \dots, \phi_M]^T \right)^{-1} \phi_j \right]^{-1} \right] \quad (56)$$

$$\approx C_j^+ \equiv \mathbb{E}_{\{\phi_k\}_{k=1}^M, \tilde{\phi}_j} \left[\left[\phi_j^T \left([\phi_1, \dots, \phi_{j-1}, \tilde{\phi}_j, \phi_{j+1}, \dots, \phi_M] \mathbf{\Lambda} [\phi_1, \dots, \phi_{j-1}, \tilde{\phi}_j, \phi_{j+1}, \dots, \phi_M]^T \right)^{-1} \phi_j \right]^{-1} \right]. \quad (57)$$

We now compare Equations 54 and 57. Each is an expectation over $M + 1$ vectors from the isotropic measure with the constraint that, when stacked, they form a design matrix Φ such that $\Phi^T \Phi = (M + 1) \mathbf{I}_n$. Though they are not independent, the statistics of these $M + 1$ vectors are symmetric under exchange, so we are free to relabel them. Equation 54 is identical to Equation 57 upon relabeling $\phi_i \rightarrow \phi_j$, $\tilde{\phi}_i \rightarrow \phi_i$, and $\phi_j \rightarrow \tilde{\phi}_j$, so they are equivalent, and $C_i^+ = C_j^+$. This in turn implies that $C_i \approx C_j$.

In light of this, we now replace all C_i with a mode-independent (but as-of-yet-unknown) constant C . This argument is closely related to the cavity method of statistical physics (Del Ferraro et al., 2014), which we expect could be applied to further develop the approximate theory we present in this work.

E.4. Fixing the Constant C

We can determine the value of C by observing that, using the ridgeless case of Theorem 3.2,

$$\sum_i \mathbb{E} [\mathbf{T}_{ii}^{(\mathcal{D})}] = \sum_i \frac{\lambda_i}{\lambda_i + C} = n. \quad (58)$$

E.5. Differentiating w.r.t. $\mathbf{\Lambda}$ to Obtain the Covariance

Here we derive expressions for the second-order statistics of $\mathbf{T}^{(\mathcal{D})}$. These derivations make no further approximations beyond those already made in approximating $\mathbb{E} [\mathbf{T}^{(\mathcal{D})}]$. We begin with a calculation that will later be of use: differentiating both sides of the constraint on C with respect to a particular eigenvalue, we find that

$$\frac{d}{d\lambda_i} \sum_{j=1}^M \frac{\lambda_j}{\lambda_j + C} = \sum_{j=1}^M \frac{-\lambda_j}{(\lambda_j + C)^2} \frac{dC}{d\lambda_i} + \frac{C}{(\lambda_i + C)^2} = 0, \quad (59)$$

yielding that

$$\frac{dC}{d\lambda_i} = \frac{C}{q(\lambda_i + C)^2}, \quad \text{where } q \equiv \sum_{j=1}^M \frac{\lambda_j}{(\lambda_j + C)^2}. \quad (60)$$

We now factor $\mathbf{T}^{(\mathcal{D})}$ into two matrices as

$$\mathbf{T}^{(\mathcal{D})} = \mathbf{\Lambda} \mathbf{Z}, \quad \text{where } \mathbf{Z} \equiv \Phi (\Phi^T \mathbf{\Lambda} \Phi)^{-1} \Phi^T. \quad (61)$$

Unlike $\mathbf{T}^{(\mathcal{D})}$, the matrix \mathbf{Z} has the advantage of being symmetric and containing only one factor of $\mathbf{\Lambda}$. Our approach will be to study the second-order statistics of \mathbf{Z} , which will trivially give these statistics for $\mathbf{T}^{(\mathcal{D})}$. Examining our expression for $\mathbb{E} [\mathbf{T}^{(\mathcal{D})}]$, we find that the expectation of \mathbf{Z} is

$$\mathbb{E} [\mathbf{Z}] = (\mathbf{\Lambda} + C \mathbf{I}_M)^{-1}. \quad (62)$$

We also define a modified \mathbf{Z} -matrix $\mathbf{Z}^{(\mathbf{U})} \equiv \Phi (\Phi^T \mathbf{U}^T \Lambda \mathbf{U} \Phi)^{-1} \Phi^T$, where \mathbf{U} is an orthogonal $M \times M$ matrix. Because the measure over which Φ is averaged is rotation-invariant, we can equivalently average over $\tilde{\Phi} \equiv \mathbf{U} \Phi$ with the same measure, giving

$$\mathbb{E}_{\Phi} [\mathbf{Z}^{(\mathbf{U})}] = \mathbb{E}_{\tilde{\Phi}} \left[\mathbf{U}^T \tilde{\Phi} \left(\tilde{\Phi}^T \Lambda \tilde{\Phi} \right)^{-1} \tilde{\Phi}^T \mathbf{U} \right] = \mathbb{E}_{\Phi} [\mathbf{U}^T \mathbf{Z} \mathbf{U}] = \mathbf{U}^T (\Lambda + C \mathbf{I}_M)^{-1} \mathbf{U}. \quad (63)$$

It is similarly the case that

$$\mathbb{E}_{\Phi} \left[(\mathbf{Z}^{(\mathbf{U})})_{ij} (\mathbf{Z}^{(\mathbf{U})})_{k\ell} \right] = \mathbb{E}_{\Phi} \left[(\mathbf{U}^T \mathbf{Z} \mathbf{U})_{ij} (\mathbf{U}^T \mathbf{Z} \mathbf{U})_{k\ell} \right]. \quad (64)$$

Our aim will be to calculate expectations of the form $\mathbb{E}_{\Phi} [\mathbf{Z}_{ij} \mathbf{Z}_{k\ell}]$. With a clever choice of \mathbf{U} , we can now see that most choices of the four indices will make this expression zero. We define $\mathbf{U}_{ab}^{(m)} \equiv \delta_{ab} (1 - 2\delta_{am})$ and observe that, because Λ is diagonal, $(\mathbf{U}^{(m)})^T \Lambda \mathbf{U}^{(m)} = \Lambda$ and thus $\mathbf{Z}^{(\mathbf{U}^{(m)})} = \mathbf{Z}$. Equation 64 then yields that

$$\mathbb{E}_{\Phi} [\mathbf{Z}_{ij} \mathbf{Z}_{k\ell}] = (-1)^{\delta_{im} + \delta_{jm} + \delta_{km} + \delta_{\ell m}} \mathbb{E}_{\Phi} [\mathbf{Z}_{ij} \mathbf{Z}_{k\ell}], \quad (65)$$

from which it follows that $\mathbb{E}_{\Phi} [\mathbf{Z}_{ij} \mathbf{Z}_{k\ell}] = 0$ if any index is repeated an odd number of times. In light of the fact that $\mathbf{Z}_{ij} = \mathbf{Z}_{ji}$, there are only three distinct nontrivial cases to consider:

1. $\mathbb{E}_{\Phi} [\mathbf{Z}_{ii} \mathbf{Z}_{ii}]$,
2. $\mathbb{E}_{\Phi} [\mathbf{Z}_{ij} \mathbf{Z}_{ij}]$ with $i \neq j$, and
3. $\mathbb{E}_{\Phi} [\mathbf{Z}_{ii} \mathbf{Z}_{jj}]$ with $i \neq j$.

We are not using the Einstein convention of summation over repeated indices.

Cases 1 and 2. We now consider differentiating \mathbf{Z} with respect to a particular element of the matrix Λ . This yields

$$\frac{d\mathbf{Z}_{i\ell}}{d\Lambda_{jk}} = -\phi_i^T (\Phi^T \Lambda \Phi)^{-1} \phi_j \phi_k^T (\Phi^T \Lambda \Phi)^{-1} \phi_{\ell} = -\mathbf{Z}_{ij} \mathbf{Z}_{k\ell}, \quad (66)$$

where ϕ_i is the i th row of Φ . This gives us the useful expression that

$$\mathbb{E} [\mathbf{Z}_{ij} \mathbf{Z}_{k\ell}] = -\frac{d}{d\Lambda_{jk}} \mathbb{E} [\mathbf{Z}_{i\ell}]. \quad (67)$$

We now set $\ell = i$ and evaluate this expression using Equation 62, concluding that

$$\mathbb{E} [\mathbf{Z}_{ij} \mathbf{Z}_{ij}] = \mathbb{E} [\mathbf{Z}_{ij} \mathbf{Z}_{ji}] = -\frac{d}{d\lambda_j} \left(\frac{1}{\lambda_i + C} \right) = \frac{1}{(\lambda_i + C)^2} \left(\delta_{ij} + \frac{C}{q(\lambda_j + C)^2} \right), \quad (68)$$

$$\text{Cov} [\mathbf{Z}_{ij}, \mathbf{Z}_{ij}] = \text{Cov} [\mathbf{Z}_{ij}, \mathbf{Z}_{ji}] = \frac{C}{q(\lambda_i + C)^2 (\lambda_j + C)^2}. \quad (69)$$

We did not require that $i \neq j$, and so Equation 68 holds for Case 1 as well as Case 2.

Case 3. We now aim to calculate $\mathbb{E} [\mathbf{Z}_{ii} \mathbf{Z}_{jj}]$ with $i \neq j$. We might hope to use Equation 67 in calculating $\mathbb{E} [\mathbf{Z}_{ii} \mathbf{Z}_{jj}]$, but this approach is stymied by the fact that we would need to take a derivative with respect to Λ_{ij} , but we only have an approximation for \mathbf{Z} for diagonal Λ . We can circumvent this by means of $\mathbf{Z}^{(\mathbf{U})}$. From the definition of $\mathbf{Z}^{(\mathbf{U})}$, we find that

$$\begin{aligned}
 & \left(\frac{d}{d\mathbf{U}_{ij}} - \frac{d}{d\mathbf{U}_{ji}} \right) \mathbf{Z}^{(\mathbf{U})} \Big|_{\mathbf{U}=\mathbf{I}_M} \\
 &= -\phi_i^T (\Phi^T \Lambda \Phi)^{-1} \left[\phi_j \lambda_i \phi_i^T - \phi_i \lambda_j \phi_j^T + \phi_i \lambda_i \phi_j^T - \phi_j \lambda_j \phi_i^T \right] (\Phi^T \Lambda \Phi)^{-1} \phi_j \\
 &= (\lambda_j - \lambda_i) (\mathbf{Z}_{ij}^2 + \mathbf{Z}_{ii} \mathbf{Z}_{jj}). \quad (70)
 \end{aligned}$$

Differentiating with respect to both \mathbf{U}_{ij} and \mathbf{U}_{ji} with opposite signs ensures that the derivative is taken within the manifold of orthogonal matrices. Now, using Equation 63, we find that

$$\begin{aligned}
 \left(\frac{d}{d\mathbf{U}_{ij}} - \frac{d}{d\mathbf{U}_{ji}} \right) \mathbb{E}[\mathbf{Z}^{(\mathbf{U})}] \Big|_{\mathbf{U}=\mathbf{I}_M} &= \left(\frac{d}{d\mathbf{U}_{ij}} - \frac{d}{d\mathbf{U}_{ji}} \right) \mathbf{U}^T (\Lambda + C \mathbf{I}_M)^{-1} \mathbf{U} \Big|_{\mathbf{U}=\mathbf{I}_M} \\
 &= \frac{1}{\lambda_i + C} - \frac{1}{\lambda_j + C}. \quad (71)
 \end{aligned}$$

Taking the expectation of Equations 70, plugging in Equation 68 for the squared off-diagonal element, comparing to 71, and performing some algebra, we conclude that

$$\mathbb{E}[\mathbf{Z}_{ii} \mathbf{Z}_{jj}] = \frac{1}{(\lambda_i + C)(\lambda_j + C)} - \frac{C}{q(\lambda_i + C)^2(\lambda_j + C)^2} \quad (72)$$

and that $\mathbf{Z}_{ii}, \mathbf{Z}_{jj}$ are anticorrelated with covariance

$$\text{Cov}_{\Phi}[\mathbf{Z}_{ii}, \mathbf{Z}_{jj}] = -\frac{C}{q(\lambda_i + C)^2(\lambda_j + C)^2}. \quad (73)$$

With the use of Kronecker deltas, we can combine Equations 69 and 73 into one expression covering all cases. As can be verified by case-by-case evaluation, one such expression is

$$\text{Cov}_{\Phi}[\mathbf{Z}_{ij}, \mathbf{Z}_{k\ell}] = \frac{C (\delta_{ik} \delta_{j\ell} + \delta_{i\ell} \delta_{jk} - \delta_{ij} \delta_{k\ell})}{q(\lambda_i + C)(\lambda_j + C)(\lambda_k + C)(\lambda_{\ell} + C)}. \quad (74)$$

Using the fact that $\mathbf{T}_{ij}^{(\mathcal{D})} = \lambda_i \mathbf{Z}_{ij}$, defining $\mathcal{L}_i \equiv \lambda_i(\lambda_i + C)$, and noting that $q = \sum_i \mathcal{L}_i(1 - \mathcal{L}_i)$, we obtain the elementwise covariances of $\mathbf{T}^{(\mathcal{D})}$ reported in Theorem 4.1.

E.6. Adding Back the Ridge Parameter

Our approximate results have thus far all assumed $\delta = 0$, which has simplified our derivations. We can now add the ridge parameter back with the observation of Appendix E that the ridge parameter can be viewed essentially as a uniform increase in all eigenvalues. To reiterate, letting $\mathbf{T}^{(\mathcal{D})}(\Lambda; \delta)$ denote the learning transfer matrix with eigenvalue matrix Λ and ridge parameter δ , it holds that $\Phi^T \Phi = M \mathbf{I}_n$ that

$$\mathbf{T}^{(\mathcal{D})}(\Lambda; \delta) = \frac{\Lambda}{\Lambda + \frac{\delta}{M} \mathbf{I}_M} \mathbf{T}^{(\mathcal{D})} \left(\Lambda + \frac{\delta}{M} \mathbf{I}_M; 0 \right). \quad (75)$$

To add a ridge parameter, then, we need merely replace $\lambda_i \rightarrow \lambda_i + \frac{\delta}{M}$ and then multiply $\mathbf{T}_{ij}^{(\mathcal{D})}$ by $\lambda_i(\lambda_i + \frac{\delta}{M})^{-1}$. This yields that

$$\mathbb{E}[\mathbf{T}_{ii}^{(\mathcal{D})}] = \frac{\delta_{ij}\lambda_i}{\lambda_i + \frac{\delta}{M} + C}, \quad (76)$$

$$\text{Cov}[\mathbf{T}_{ij}^{(\mathcal{D})}, \mathbf{T}_{k\ell}^{(\mathcal{D})}] = \frac{C(\delta_{ik}\delta_{j\ell} + \delta_{i\ell}\delta_{jk} - \delta_{ij}\delta_{k\ell})}{q(\lambda_i + \frac{\delta}{M} + C)(\lambda_j + \frac{\delta}{M} + C)(\lambda_k + \frac{\delta}{M} + C)(\lambda_\ell + \frac{\delta}{M} + C)}, \quad (77)$$

$$\text{where } C \geq 0 \text{ satisfies } \sum_i \frac{\lambda_i + \frac{\delta}{M}}{\lambda_i + \frac{\delta}{M} + C} = n \text{ and } q \equiv \sum_{j=1}^M \frac{\lambda_j + \frac{\delta}{M}}{(\lambda_j + \frac{\delta}{M} + C)^2}. \quad (78)$$

Taking $M \rightarrow \infty$, we find that

$$\mathbb{E}[\mathbf{T}_{ii}^{(\mathcal{D})}] = \frac{\delta_{ij}\lambda_i}{\lambda_i + C}, \quad (79)$$

$$\text{Cov}[\mathbf{T}_{ij}^{(\mathcal{D})}, \mathbf{T}_{k\ell}^{(\mathcal{D})}] = \frac{C(\delta_{ik}\delta_{j\ell} + \delta_{i\ell}\delta_{jk} - \delta_{ij}\delta_{k\ell})}{q(\lambda_i + C)(\lambda_j + C)(\lambda_k + C)(\lambda_\ell + C)}, \quad (80)$$

$$\text{where } C \geq 0 \text{ satisfies } \sum_i \frac{\lambda_i}{\lambda_i + C} + \frac{\delta}{C} = n \text{ and } q \equiv \sum_{j=1}^M \frac{\lambda_j}{(\lambda_j + C)^2} + \frac{\delta}{C^2}. \quad (81)$$

These expressions, which reduce to those for finite M when $\delta = 0$, are equivalent to those given in Theorem 4.1.

E.7. Target Noise

Suppose that, instead of given clean targets, we are given noisy labels $f^*(x_i) + \eta_i$, where f^* is the noiseless underlying function and $\eta_i \sim \mathcal{N}(0, \epsilon^2)$ is the noise when the function is evaluated on x_i . As long as we are assured that no input will either appear twice in the training set or appear in both the training and test sets, instead of viewing the noise as a random variable sampled with each function evaluation, we can instead view it as a random but fixed noisy perturbation to f which alters its eigencoefficients to be $\mathbf{v} \rightarrow \mathbf{v}^* + \tilde{\mathbf{v}}$, where \mathbf{v}^* are the original coefficients and the elements of $\tilde{\mathbf{v}}$ are sampled i.i.d from $\mathcal{N}(0, \frac{\epsilon^2}{M})$. We can then examine the statistics of \hat{f} when trained on this noisy function.

In the $M \rightarrow \infty$ limit, all the noise is in arbitrarily low eigenmodes with $\mathcal{L}_i = 0$. In this limit, the expected learnability observed when fitting a noisy function is

$$\mathcal{L}(f) = \mathbb{E} \left[\frac{\hat{\mathbf{v}}^T \mathbf{v}}{\mathbf{v}^T \mathbf{v}} \right] = \frac{(\mathbf{v}^*)^T \mathbb{E}[\mathbf{T}^{(\mathcal{D})}] \mathbf{v}^*}{(\mathbf{v}^*)^T \mathbf{v}^* + \epsilon^2} = \frac{\|f^*\|_2^2}{\|f^*\|_2^2 + \epsilon^2} \mathcal{L}(f^*). \quad (82)$$

Observed learnability is thus lowered with the addition of noise. That said, the expected unnormalized inner product of \hat{f} with the true function (i.e., $\mathbb{E}[\hat{\mathbf{v}}^T \mathbf{v}^*]$) remains unchanged. In this limit, MSE becomes

$$\mathcal{E}(f) = \frac{n}{n - \sum_m \mathcal{L}_m^2} \left(\sum_i (1 - \mathcal{L}_i)^2 \mathbf{v}_i^2 + \epsilon^2 \right). \quad (83)$$

The covariance of the predicted coefficients in the case of noise is still given by Equation 16 using the noisy MSE.

E.8. Properties of C

In experimental settings, C is in general easy to find numerically, but for theoretical study, we anticipate it being useful to have some analytical bounds on C in order to, for example, prove that certain eigenmodes are or are not asymptotically learned for particular spectra. To that end, the following lemma gives some properties of C .

Lemma E.1. *For $C \geq 0$ solving $\sum_{i=1}^M \frac{\lambda_i}{\lambda_i + C} + \frac{\delta}{C} = n$, with positive eigenvalues $\{\lambda_i\}_{i=1}^M$ ordered from greatest to least, the following properties hold:*

(a) $C = \infty$ when $n = 0$, and $C = 0$ when $n \rightarrow M$ and $\delta = 0$.

(b) C is strictly decreasing with n .

(c) $C \leq \frac{1}{n-\ell} \left(\delta + \sum_{i=\ell+1}^M \lambda_i \right)$ for all $\ell \in \{0, \dots, n-1\}$.

(d) $C \geq \lambda_\ell \left(\frac{\ell}{n} - 1 \right)$ for all $\ell \in \{n, \dots, M\}$.

Proof of property (a): Because $\sum_{i=1}^M \frac{\lambda_i}{\lambda_i + C} + \frac{\delta}{C}$ is strictly decreasing with C for $C \geq 0$, there can only be one solution for a given n . The first statement follows by inspection, and the second follows by inspection and our assumption that all eigenvalues are strictly positive.

Proof of property (b): Differentiating the constraint on C with respect to n yields

$$\left[\sum_{i=1}^M \frac{-\lambda_i}{(\lambda_i + C)^2} + \frac{-\delta}{C^2} \right] \frac{dC}{dn} = 1, \quad \text{which implies that} \quad \frac{dC}{dn} = - \left[\sum_{i=1}^M \frac{\lambda_i}{(\lambda_i + C)^2} + \frac{\delta}{C^2} \right]^{-1} < 0. \quad (84)$$

Proof of property (c): We observe that $n = \sum_{i=1}^M \frac{\lambda_i}{\lambda_i + C} + \frac{\delta}{C} \leq \ell + \sum_{i=\ell+1}^M \frac{\lambda_i}{C} + \frac{\delta}{C}$. The desired property follows.

Proof of property (d): We set $\delta = 0$ and consider replacing λ_i with λ_ℓ if $i \leq \ell$ and 0 if $i > \ell$. Noting that this does not increase any term in the sum, we find that $n = \sum_{i=1}^M \frac{\lambda_i}{\lambda_i + C} \geq \sum_{i=1}^\ell \frac{\lambda_\ell}{\lambda_\ell + C} = \frac{\ell \lambda_\ell}{\lambda_\ell + C}$. The desired property in the ridgeless case follows. A positive ridge parameter only increases C , so the property holds in general. We note that a positive ridge parameter can be incorporated into the bound, giving

$$C \geq \frac{1}{2n} \left[(\ell - n)\lambda_\ell + \delta + \sqrt{((\ell - n)\lambda_\ell + \delta)^2 + 4n\delta\lambda_\ell} \right]. \quad \square \quad (85)$$

We also note that, as observed by [Jacot et al. \(2020\)](#) and [Spigler et al. \(2020\)](#), the asymptotic scaling of C can be fixed if the kernel eigenvalues follow a power law spectrum. Specifically, if $\lambda_i \sim i^{-\alpha}$ for some $\alpha > 1$, then [Jacot et al. \(2020\)](#)⁹ show that

$$C = \Theta(\delta n^{-1} + n^{-\alpha}). \quad (86)$$

⁹[Jacot et al. \(2020\)](#) scale the ridge parameter proportional to n in their definition of kernel ridge regression; our reproduction of their result accounts for this and applies to our convention.